Annu. Rev. Nucl. Part. Sci. 2005. 55:271–310
doi: 10.1146/annurev.nucl.55.090704.151526

PHYSICS OF ULTRA-PERIPHERAL NUCLEAR COLLISIONS

Carlos A. Bertulani,[1] Spencer R. Klein,[2] and Joakim Nystrand[3]

[1]*Department of Physics, University of Arizona, Tucson, Arizona 85721; email: bertulani@physics.arizona.edu*

[2]*Nuclear Science Division, Lawrence Berkeley National Laboratory, Berkeley, California, 94720; email: srklein@lbl.gov*

[3]*Department of Physics and Technology, University of Bergen, 5007 Bergen, Norway; email: joakim.nystrand@ift.uib.no*

Key Words nuclear collisions, relativistic, heavy ions, virtual photons, particle production, nuclear fragmentation, two-photon reactions, photonuclear reactions

■ **Abstract** Moving highly-charged ions carry strong electromagnetic fields that act as a beam of photons. In collisions at large impact parameters, hadronic interactions are not possible, and the ions interact through photon-ion and photon-photon collisions known as ultra-peripheral collisions (UPCs). Hadron colliders like the Relativistic Heavy Ion Collider (RHIC), the Tevatron, and the Large Hadron Collider (LHC) produce photonuclear and two-photon interactions at luminosities and energies beyond that accessible elsewhere; the LHC will reach a γp energy ten times that of the Hadron-Electron Ring Accelerator (HERA). Reactions as diverse as the production of anti-hydrogen, photoproduction of the ρ^0, transmutation of lead into bismuth, and excitation of collective nuclear resonances have already been studied. At the LHC, UPCs can study many types of new physics processes.

CONTENTS

1. INTRODUCTION

In 1924, Enrico Fermi, then 23 years old, submitted a paper "On the Theory of Collisions Between Atoms and Elastically Charged Particles" to Zeitschrift für Physik (1). This paper does not appear in his "Collected Works." Nevertheless, it is said that this was one of Fermi's favorite ideas and that he often used it later in life (2). In this publication, Fermi devised a method known as the equivalent (or virtual) photon method, where he treated the electromagnetic fields of a charged particle as a flux of virtual photons. Ten years later, Weiszsäcker and Williams extended this approach to include ultra-relativistic particles, and the method is often known as the Weizsäcker-Williams method (3).

A fast-moving charged particle has electric field vectors pointing radially outward and magnetic fields circling it. The field at a point some distance away from the trajectory of the particle resembles that of a real photon. Thus, Fermi replaced the electromagnetic fields from a fast particle with an equivalent flux of photons. The number of photons with energy ω, $n(\omega)$, is given by the Fourier transform of the time-dependent electromagnetic field. The virtual photon approach used in quantum electrodynamics (QED) to describe, e.g., atomic ionization or nuclear excitation by a charged particle, can be simply described using Fermi's approach.

When two nuclei collide, two types of electromagnetic processes can occur. A photon from one ion can strike the other, Figure 1*a*, or, photons from each nucleus can collide, in a photon-photon collision, as in Figure 1*b*.

Ultra-peripheral hadron-hadron collisions will provide unique opportunities for studying electromagnetic processes. At the Large Hadron Collider (LHC), photon-proton collisions will occur at center of mass energies an order of magnitude higher than are available at existing accelerators, and photon-heavy ion collisions will reach 30 times the energies available at fixed target accelerators. The electromagnetic fields of heavy ions are very strong, so reactions involving multi-photon excitations can be studied.

Ultra-relativistic heavy-ion interactions have been used to study nuclear photoexcitation (e.g., to a Giant Dipole Resonance) and photoproduction of hadrons. Coulomb excitation is a traditional tool in low-energy nuclear physics. The strong electromagnetic fields from a heavy ion allow for the study of multi-photon excitation of nuclear targets. This can produce high-lying states in nuclei, e.g., the double-giant resonance (4, 5). Multiple, independent interactions among a single ion pair are also possible. Reactions like multiple vector meson production can

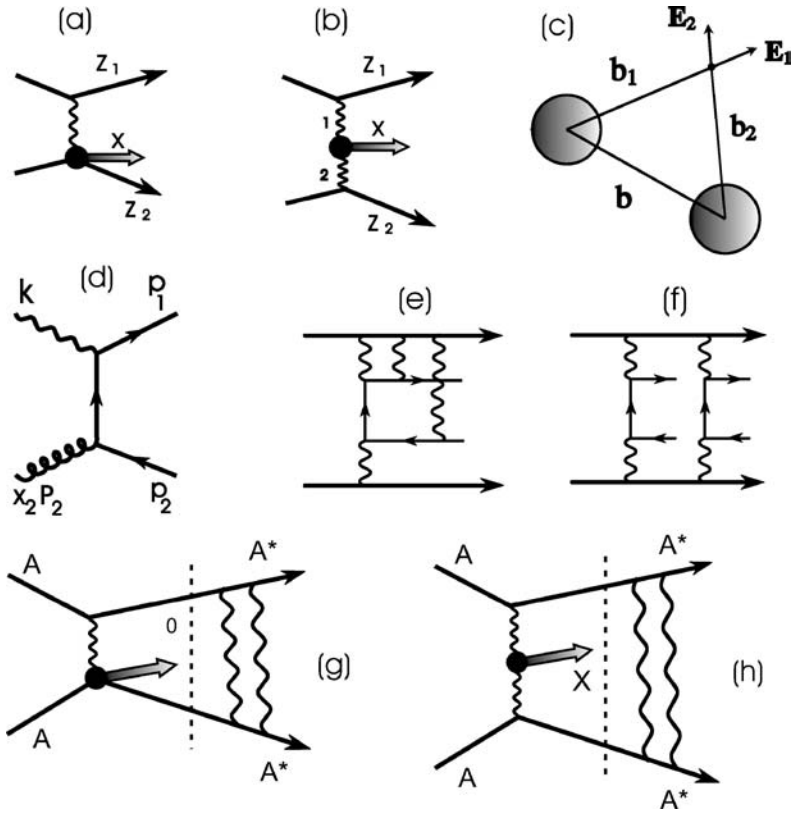

Figure 1 (*a*) One-photon and (*b*) two-photon processes in heavy ion collisions. (*c*) Geometrical representation of the photon fluxes at a point outside nuclei 1 and 2, in a collision with impact parameter *b*. The electric field of the photons at that point are also shown. (*d*) Feynman diagram for $q\overline{q}$ production through photon-gluon fusion to leading order. (*e*, *f*) Example of higher order corrections to pair production: (*e*) Coulomb distortion, and (*f*) production of multiple pairs. (*g*) The dominant diagram for Au+Au $\rightarrow$ Au*+ Au*+ ρ^0 and (*h*) for Au+Au $\rightarrow$ Au*+Au* + e^+e^- or a meson *X*. The dotted lines in panels (*g*) and (*h*) show how the mutual Coulomb nuclear excitation factorizes from the particle production.

be used for studies involving polarized photons. The high photon energies can be used to study the gluon density in heavy nuclei (6) at low Feynman-*x*.

The cross section for photoproduction of a state *x* is

$$\sigma_X = \int d\omega \frac{n(\omega)}{\omega} \sigma_X^{\gamma}(\omega), \qquad 1.$$

where $\sigma_X^{\gamma}(\omega)$ is the photonuclear cross section.

Photon-photon (or two-photon) processes have long been studied at e^+e^- colliders. They are an excellent tool for many aspects of meson spectroscopy and

tests of QED. At hadron colliders, they are also used to study atomic physics processes, often involving electrodynamics in strong fields. One striking success was the production of antihydrogen atoms at CERN's[1] LEAR[2] (7) and at the Fermilab Tevatron (8). At the highest energy colliders, reactions like $\gamma\gamma \to X$ may be used to probe the quark content and spin structure of meson resonances. Production of meson or baryon pairs can also probe the internal structure of hadrons. At the LHC, electroweak processes such as $\gamma\gamma \to W^+W^-$ may be probed. The cross section for two-photon processes is (9)

$$\sigma_X = \int d\omega_1 \; d\omega_2 \frac{n(\omega_1)}{\omega_1} \frac{n(\omega_2)}{\omega_2} \sigma_X^{\gamma\gamma}(\omega_1, \omega_2), \qquad 2.$$

where $\sigma_X^{\gamma\gamma}(\omega_1, \omega_2)$ is the two-photon cross section.

Fermi's method has found application beyond the realms of QED. It has been extended to strong interactions between nuclei in peripheral collisions. These interactions are mainly mediated by pion exchange, and an equivalent pion method has been applied to describe subthreshold pion production in nucleus-nucleus collisions (10). Feshbach used the term nuclear Weiszsäcker-Williams method to describe excitation processes induced by the nuclear interaction in peripheral collisions of heavy ions (11). More recently, a non-Abelian Weiszsäcker-Williams field was used to describe the boosted gluon distribution functions in nuclear collisions (12).

Since Fermi's original work, much progress has been achieved in this field, especially with the advent of relativistic heavy-ion accelerators like the Bevalac accelerator at Lawrence Berkeley National Laboratory (LBNL). Intermediate energy processes have been explored at heavy-ion accelerators at NSCL/MSU, GANIL, RIKEN, and GSI[3]; these facilities have explored the collective excitation and electromagnetic fragmentation of nuclei and studied many reactions that occur in the sun, supernovae, and the big bang. Experimental studies of higher-energy processes have recently begun at Brookhaven's RHIC. In the next few years, CERNs LHC will begin operations, allowing for the study of heavy mesons, measurements of gluon distributions in nuclei, and searches for a host of new physics processes.

This review will discuss these experiments, their theoretical interpretation, and some future possibilities in this field. UPCs have been previously reviewed by a number of authors (9, 13–16).

[1]European Organization for Nuclear Research (Conseil Européenne pour la Recherche Nucléaire).

[2]Low Energy Antiproton Ring.

[3]NSCL/MSU: National Science Cyclotron Laboratory at Michigan State University, GANIL: Grand Accelerateur National d'Ions Lourds in Caen/France, RIKEN: The Institute of Physical and Chemical Research, Wako, Saitama/Japan, GSI: Gesellschaft fuer Schwerionenforschung, Darmstadt/Germany.

1.1. The Photon Flux

The flux of equivalent photons from a charged particle is determined from the Fourier transform of the electromagnetic field of the moving charge. The fields of a relativistic particle Lorentz contract toward a co-moving pancake (see Figure 2). The photon energy spectrum depends on the time a target particle spends in this pancake, i.e., on the minimum distance between the target and the charge and on the projectile velocity; the minimum photon wavelength is the width of the pancake at the target. At an ion-ion separation (impact parameter) b, the interaction time is $\Delta t \sim \mathrm{b}/(\gamma v)$. In the lab frame, the maximum photon energy is

$$\omega^{\max} = \frac{\hbar}{\Delta t} \sim \frac{\gamma \hbar v}{b}, \qquad 3.$$

where γ is the Lorentz factor of the particle, $\gamma = (1 - v^2/c^2)^{-1/2}$. In the target frame, this equation applies, as long as γ is taken as the boost to go from the frame of one nucleus to the other ($\gamma = 2\gamma^2_{collider} - 1$).

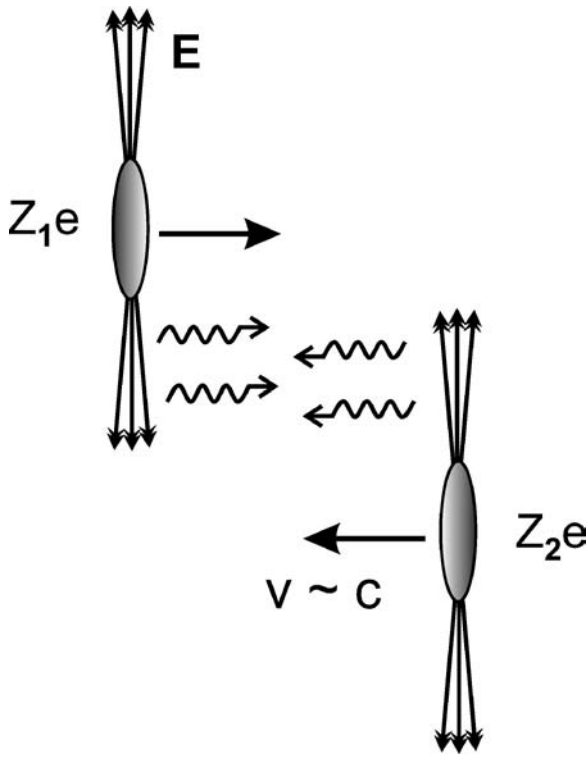

Figure 2 Highly energetic charges have Lorentz contracted electric (and magnetic) fields. The interaction between these fields can be replaced by the interaction of real (or quasi-real) photons.

For a grazing collision, where the two nuclei barely touch, we can take $b_{min} = 2R_A$, and the maximum photon energy is $\gamma\hbar v/2R_A$ (R_A = nuclear radius). The maximum photon energy is about $\hbar/(2R_A A m_p c)$ of the ion energy. Here, Am_p is the ion mass. For heavy ions, $R_A \approx 7$ fm so ω^{max} is about $0.03/A$ of the ion energy. For protons, R_A is not well defined, but taking ω^{max} to be 10% of the proton energy is a reasonable rule of thumb. RHIC (see Table 1) can reach photon-gold center of mass energies up to about 30 GeV per nucleon, and photon-proton center of mass energies up to 300 GeV. These energies are slightly higher than are available at fixed target accelerators and at HERA respectively. At the LHC, the corresponding energies are 1 TeV and 10 TeV respectively, more than an order of magnitude higher than is available elsewhere.

The equivalent (or virtual) photon flux per unit area (the relation between $n(\omega)$ and $N(\omega, b)$) is $n(\omega) = \int N(\omega, b)\, d^2b)$ is (1, 3, 17)

$$N(\omega, b) = \frac{Z^2\alpha\omega^2}{\pi^2\gamma^2\hbar^2\beta^2c^2}\left(K_1^2(x) + \frac{1}{\gamma^2}K_0^2(x)\right). \qquad 4.$$

where $x = \omega b/\gamma\beta\hbar c$, Z is the ion charge, $\alpha = 1/137$, βc is the particle velocity, and K_0 and K_1 are modified Bessel functions. The first term $(K_1(x)^2)$ gives the flux of photons transversely polarized to the ion direction and the second is the flux for longitudinally polarized photons. The transverse polarization dominates for ultra-relativistic particles ($\gamma \gg 1$). The photon flux is exponentially suppressed when $\omega > \gamma\beta\hbar c/b$, justifying the estimates in the beginning of this section.

These photons are almost real, with virtuality $-q^2 < (\hbar/R_A)^2$. Except for the production of e^+e^- pairs, the photons can usually be treated as real photons.

The usable photon flux depends on the geometry. Most UPC reactions lead to final states with a handful of particles. These final states will be overwhelmed by any

TABLE 1 Some ion species, maximum energy and luminosity for several accelerators (170). Also shown are the maximum effective γp and $\gamma\gamma$ energies. For photon beams, the maximum effective photon energy here is 10% of the proton energy; there is some flux at higher energies. The CERN SPS is a fixed target accelerator; the effective luminosity depends on the target thickness. Not mentioned here are lower-energy accelerators, where photon exchange processes have also been studied.

Accelerator	Ions	Max. Energy per nucleon pair (CM)	Luminosity	Max. γp	Max. $\gamma\gamma$ energy
CERN SPS	Pb+Pb	17 GeV	—	3.1 GeV	0.8 GeV
RHIC	Au+Au	200 GeV	4×10^{26} cm^{-2} s^{-1}	24 GeV	6.0 GeV
RHIC	p+p	500 GeV	6×10^{30} cm^{-2} s^{-1}	79 GeV	50 GeV
LHC	Pb+Pb	5.6 TeV	10^{27} cm^{-2} s^{-1}	705 GeV	178 GeV
LHC	p+p	14 TeV	10^{34} cm^{-2} s^{-1}	3130 GeV	1400 GeV
Tevatron	p+$\bar{\text{p}}$	20 TeV	5×10^{31} cm^{-2} s^{-1}	320 GeV	200 GeV

hadronic interactions between the fast-moving ion and the target. Thus, the useful photon flux is that for which the ions do not overlap, i.e., when the impact parameter $b = |\mathrm{b}_1 - \mathrm{b}_2|$ is greater than twice the nuclear radius ($2R_A$) (see Figure 1*c*). Usually, we can take $R_A = 1.2\,A^{1/3}$ fm, where A is the atomic number. The $b > 2R_A$ requirement treats the nuclei as hard spheres; it is accurate for heavy nuclei, but less appropriate for lighter ions.

The photons can interact with a target nucleus in a one-photon process (when $b_1 < R_A$) or with its electromagnetic field in a two-photon process (when $b_1 > R_A$ and $b_2 > R_A$). In a photonuclear (one-photon) interaction, the usable photon flux is obtained by integrating Equation 4 over $b > b_{min} = 2R_A$:

$$n(\omega) = \frac{2Z^2\alpha}{\pi\beta^2}\left[\xi K_0(\xi)K_1(\xi) - \frac{\xi^2}{2}\left(K_1^2(\xi) - K_0^2(\xi)\right)\right] \qquad 5.$$

where $\xi = \omega b_{min}/\gamma\beta\hbar c = 2\,\omega\,R_\mathrm{A}/\gamma\beta\hbar c$.

For two-photon exchange processes, the equivalent photon numbers in Equation 2 must account for the electric field orientation of the photon fluxes with respect to each ion (see Figure 1*b*), obeying the ion non-overlap criteria $b_1, b_2 > R_A$ (14). The effects of orientation are also not included in Equation 5. For instance, symmetry properties dictate that $J^\pi = 0^+$ (scalar) particles originate from configurations such that $\mathrm{E}_1 \parallel \mathrm{E}_2$, whereas 0^- (pseudo-scalar) particles originate from $\mathrm{E}_1 \perp \mathrm{E}_2$ (18, 19). If one uses Equation 5 for $n(\omega_1)$ and $n(\omega_2)$, the total photoproduction cross section obtained from Equation 2 is higher than in a more detailed calculation, and the difference increases with increasing particle masses (18). Even more detailed calculations can be done by replacing the sharp-cutoff, $b_1, b_2 > R_A$, criterion with integrals over b_1 and b_2, which are weighted by the hadronic non-interaction probability. Asymmetric collisions (especially *pA* and *dA*) are also of interest; the higher-*Z* nucleus is likely to be the photon emitter, so the photon direction is known.

Low-energy processes, e.g., nuclear excitation, are also sensitive to the electromagnetic multipolarity involved. Equations 4 and 5 are only appropriate for electric dipole (E1) excitations. Equations for higher multipolarities are described in Reference (9).

For protons, the hard sphere approximation is inadequate. Instead, the proton size is included by the use of a form factor. With a dipole form factor, the flux is (20)

$$n(\omega) = \frac{\alpha}{2\pi z}[1 + (1-z)^2]\left(\ln\chi - \frac{11}{6} + \frac{3}{\chi} - \frac{3}{2\chi^2} + \frac{1}{3\chi^3}\right) \qquad 6.$$

where

$$\chi = 1 + \frac{0.71\ \mathrm{GeV}^2}{Q_{min}^2 c^2} \qquad 7.$$

accounts for the proton structure and $z = W^2/s$, with W the γp center of mass energy, and s the squared ion-ion center of mass energy per-nucleon. Here, Q_{min}

is the minimum momentum transfer possible in the reaction. For proton-proton collisions, the form factor has an effect similar to imposing a requirement $b_{min} = 0.7$ fm (21).

For protons and light nuclei, the weak electromagnetic interactions introduce another complication. The momentum transfer due to elastic scattering, $\Delta p = 2\eta\hbar/b$, with $\eta = Z_1 Z_2 \alpha \ll 1$ is small enough that the impact parameter is not a well-defined observable because $\Delta p \Delta b \sim \hbar$, leading to $\Delta b > b$ for $\eta < 1$ (22). This does not affect the total photon flux. However, it might affect the component of the photon flux that is unaccompanied by hadronic interactions. The uncertainty may also affect the probabilities for multiple interactions discussed in Section 5.

Equation 6 is valid when the proton remains intact. When photon emission with proton excitation, such as to the Δ resonance, is included, then the flux increases about 30% (23). At very high photon energy ($z \to 1$), the magnetic form factor of the proton can also become important (24).

1.2. Experimental Characterization

Ultra-peripheral collisions look very different from the more conventional hadronic interactions. The final state multiplicity is much smaller, and usually the events are fully reconstructed. Because the photon p_T are both small (roughly, $p_T \approx \omega/\gamma c$) in two-photon interactions, the final state p_T will be small. Photonuclear interactions that involve coherent scattering from the target nucleus (such as vector meson production) also have a very small p_T: $p_T < \hbar/R_A$. This gives the events a distinctive experimental signature, greatly simplifying detection (25).

UPCs are studied at a variety of accelerators. The characteristics of some relevant accelerators are given in Table 1. Each accelerator can accelerate many different species; Table 1 gives only a few candidates. The CERN Super Proton Synchrotron (SPS) has produced results on lead-to-bismuth transmutation and e^+e^- pair production in ion-ion collisions.

Although RHIC only began taking data in 2000, it has already released UPC results on ρ^0 photoproduction and on e^+e^- pair production. RHIC has enough energy and luminosity to photoproduce a wide variety of mesons, including the J/ψ. However, because it is a collider, detection of very low p_T particles is difficult, complicating the study of e^+e^- pairs and other atomic phenomena.

Although it is exclusively a $\overline{p}p$ collider, the Fermilab Tevatron is an interesting place to study UPCs. Antihydrogen was produced there using the process $\gamma\gamma \to e^+e^-$, with the positron bound to an antiproton (8). Photoproduction of the J/ψ (21) may have been observed by the CDF collaboration (26).

The Large Hadron Collider (LHC), scheduled to begin operation in 2007, will search for physics beyond the standard model. A UPC program at the LHC can contribute to this search. Especially for pp collisions, where $\gamma\gamma$ and γp energies up to about 10% of the beam energy are accessible, UPCs may be an attractive

place to search for new physics. With ion beams, the photon energies are lower, but $W^{\pm}$, Z, and heavy quark physics may be studied.

2. LOW-ENERGY PHOTONUCLEAR INTERACTIONS

Relativistic Coulomb Excitation (RCE) is now a popular tool to investigate the intrinsic nuclear dynamics and structure of the colliding nuclei. It is especially important in reactions involving radioactive nuclear beams (27–33), and has been used for many decades in low-energy nuclear collisions to study nuclear structure (34). However, nuclear-induced processes may also contribute to the reactions being studied.

RCE may involve single or multiple photon exchange between the projectile and the target. In the first case, perturbation theory directly relates the data to the matrix elements of electromagnetic transitions. These matrix elements are clean probes of the nuclear structure, and RCE can be used to study short-lived unstable nuclei that cannot be probed with real photons or electron scattering (28, 31, 33).

Radiative capture processes ($b + c \rightarrow a + \gamma$) play a major role in astrophysical sites, e.g., in a pre-supernova (35, 36). Some reactions of interest for astrophysics, e.g., ^{7}Be$(p, \gamma)^{8}$B, can be studied via the inverse photo-dissociation reaction ^{8}B$(\gamma, p)^{7}$Be (37) using relativistic Coulomb collisions. The Coulomb breakup reaction $a + A \rightarrow b + c + A$ is useful to obtain the corresponding γ-induced cross section $\gamma + a \rightarrow b + c$. Using detailed balance, this cross section can be related to the radiative capture cross section $b + c \rightarrow a + \gamma$, of astrophysical interest (37). The radiative capture cross sections are often expressed in terms of the astrophysical S-factor: $S(E) = \sigma(E)\ \exp(-2\pi Z_b Z_c e^2/\hbar v_{bc})/E$, where $E \equiv E_{rel} = m_{bc} v_{bc}^2/2$ is the relative energy between b and c. In this equation v_{bc} is the relative velocity and $m_{bc} = m_b m_c/(m_b + m_c)$ is the reduced mass of $b + c$. Because the Coulomb penetration factor is explicitly factored out, the S-factor is a much flatter function of E than $\sigma(E)$, allowing a better extrapolation of the measurements.

As an example, Figure 3*a* shows the result of an experiment performed at the GSI laboratory in Darmstadt, Germany (38) for the Coulomb dissociation of ^{8}B. Data on the reaction $^{7}\text{Be} + p \rightarrow \gamma + {}^{8}\text{B}$ is important for understanding the structure of our sun. The decay of ^{8}B is responsible for the high-energy neutrinos observed by earth-bound detectors. The measured S-factor (S_{17}, 1 = proton, 7 = ^{7}Be) is shown in Figure 3*a* as solid circles. The solid curve is a fit using a theoretical model for $S_{17}(E)$. Some of the data shown in the figure are from direct capture experiments (39).

Other b(c, γ) radiative capture reactions are planned or have already been studied with the Coulomb dissociation method (40). These processes may occur in the sun, supernovae, or during the Big Bang. Most of these reactions cannot be directly studied because the Coulomb barrier leads to very small values for the cross section, beyond the reach of present experimental techniques.

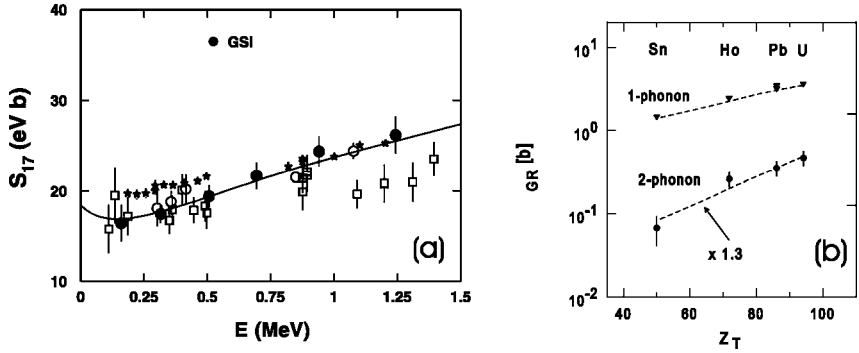

Figure 3 (*a*) S-factors (S_{17}) for the ^{7}Be(p, γ)^{8}B reaction. The GSI data was obtained using the Coulomb dissociation method (38). The other data are from direct capture measurements (39). (*b*) Cross sections for the excitation of the GDR (1-phonon) and the DGDR (2-phonon) in ^{208}Pb projectiles incident on different targets. The dashed curves are theoretical calculations.

Giant dipole resonances (GDR) occur in nuclei at energies of 10–20 MeV. Their gross properties are well described in terms of an out-of-phase collective motion (oscillation) of protons against neutrons in a nucleus (41, 42). If this oscillation is harmonic, with excitation energy $\hbar\omega$, then higher excitation modes, with energies equal to $N\hbar\omega$, also occur. These modes are interpreted as double, triple, . . . , giant dipole resonances. The double giant dipole resonances (DGDR) are thus two giant dipole vibrations superimposed in one nucleus, with about twice the energy of the GDR (4, 9, 29, 30). In the harmonic model, the RCE cross section for all multiphonon states can be calculated exactly (4).

A series of experiments at the GSI laboratory obtained the energy spectra, cross sections, and angular distribution of fragments following the decay of the DGDR (43–49). The experimental cross sections are about 30% bigger than the theoretical ones. This is shown in Figure 3*b*, where the dashed lines are the result of theoretical calculations (29, 30, 50–54). These experiments are promising for the studies of the nuclear response in very collective states. The giant resonances are still poorly understood, even with the best current microscopic approaches. The study of the width of the DGDRs will be help improve this scenario (30).

In heavy-ion colliders, the mutual Coulomb excitation of the ions (leading to their simultaneous fragmentation) is a useful tool for beam monitoring (55). A recent measurement at RHIC (56), using the Zero Degree Calorimeters to measure the neutron decay of the reaction products, has proved the feasibility of the method.

DGDRs constitute only 10% of the total fragmentation cross section induced by Coulomb excitation in UPC. The dominant contribution is the excitation of a single GDR, which then decays mostly by neutron emission. This is also a major

source of beam losses in relativistic heavy-ion colliders (57), and an important fragmentation mode of relativistic nuclei in cosmic rays.

Another useful reaction is deuteron photodissociation in d+A collisions—a photon from a heavy ion photodissociates a deuteron (58). The reaction has a large cross section, 1.38 b for d+Au at RHIC, and 2.49 b for d+Pb at the LHC (59), and has been used as a "standard candle" for luminosity monitoring (60). d+A collisions are studied because they are technically simpler than p+A collisions.

3. PHOTOPRODUCTION AT HADRON COLLIDERS

The main interest in photoproduction at hadron colliders is derived from the possibility it offers of a direct determination of the gluon distribution in nucleons and nuclei. Examples of interactions in which the gluon distribution can be probed are exclusive production of heavy vector mesons, photoproduction of heavy quark-anti-quark pairs, and photoproduction of jets. The gluon distributions are not directly accessible in deep inelastic scattering, because the gluons carry neither electrical nor weak charge.

Measuring the nuclear shadowing using heavy-ion beams is particularly interesting. The nuclear gluon density can, as a first approximation, be written as the nucleon gluon distribution, $g(x, Q^2)$, multiplied by the number of nucleons (A):

$$G^A(x, Q^2) = Ag(x, Q^2). \quad 8.$$

Here, x is the fraction of the projectile momentum carried by the gluon, and Q^2 is the 4-momentum transfer squared.

Results from deep inelastic scattering of electrons on nuclear targets have, however, showed deviations from such a simple scaling for the structure function, $F_2(x_2, Q^2)$. Depending on x, suppressions (shadowing) of up to $\sim$30% and enhancements (anti-shadowing) of up to $\sim$10% have been observed. The effects of shadowing on $G^A(x, Q^2)$ are hard to determine directly. The current best estimates of the modification to the gluon distribution in nuclei are obtained from the Q^2 evaluation of $F_2(x, Q^2)$ (61, 62) and from studies of diffractive interactions (63). Photoproduction at heavy-ion colliders may provide a more direct measurement of $G^A(x, Q^2)$.

The particle production in photon-hadron or photon-nucleus interactions can be exclusive, when the protons or nuclei remain in their ground state or are only internally excited, or inclusive, when at least one of the nucleons or nuclei breaks up. Exclusive production will be discussed first. When the momentum transfer is small compared with its inverse nucleon/nuclear size, $Q \sim \hbar c/R$, the fields couple coherently to the entire target. The kinematics of coherent, exclusive interactions is very similar to that of two-photon interactions, which will be discussed in section 4.

3.1. Exclusive Particle Production

The dominant coherent interaction leading to the production of a hadronic final state is the exclusive production of vector mesons,

$$A + A \rightarrow A + A + V. \qquad 9.$$

In these reactions, a photon from the electromagnetic field of one of the projectiles interacts coherently with the nuclear field of the other (target), producing the vector meson.

Exclusive vector meson photoproduction on proton and nuclear targets has been studied since the mid-1960s using photon beams (64) and since 1992 at the HERA electron-proton accelerator (65). The first results from a heavy-ion collider on exclusive ρ^0 production (Au+Au $\rightarrow$ Au+Au + ρ^0) were recently published by the STAR collaboration at RHIC (25).

The total vector meson cross section in p+p or A+A interactions can be calculated from Equation 1. By differentiating and changing the variable from ω to y, the rapidity of the produced vector meson, one obtains

$$\frac{d\sigma(A + A \rightarrow A + A + V)}{dy} = n(\omega)\sigma_{\gamma A \rightarrow V A}(\omega) \qquad 10.$$

where the photon energy, ω, is related to y through $\omega = (M_V c^2/2)\exp(y)$ and M_V is the mass of the vector meson. If the photon flux is known, the differential cross section, $d\sigma/dy$, is thus a direct measure of the vector meson photoproduction cross section for a given photon energy.

The bulk of the photon-hadron cross section can be explained by the photon first fluctuating to a $q\bar{q}$ pair, which interacts with the target through the strong nuclear force. Since the photon has quantum numbers $J^{PC} = 1^{--}$, it preferentially fluctuates to a vector meson. The lifetime of the fluctuation is determined by the uncertainty principle. For a photon of virtuality Q fluctuating to a state of mass M_V the lifetime is of order

$$\Delta t \approx \frac{\hbar}{\sqrt{M_V^2 c^4 + Q^2 c^2}} \approx \frac{\hbar}{M_V c^2}. \qquad 11.$$

The last approximation is always true at hadron colliders because of the low virtuality of the photons. The photon wave function is written as a Fock decomposition (66):

$$|\gamma> = C_{bare}|\gamma_{bare}> + C_\rho|\rho> + C_\omega|\omega> + C_\phi|\phi> + \cdots + C_q|q\overline{q}>. \qquad 12.$$

Here $C_{bare} \approx 1$ and $C_V \sim \sqrt{\alpha_{em}}$ ($V = \rho, \omega, \phi, \ldots$). The coefficients C_V are related to the photon-vector meson coupling, f_V, through

$$C_V = \frac{\sqrt{4\pi\alpha_{em}}}{f_V}. \qquad 13.$$

The numerical values of the couplings f_V are usually determined from the vector meson leptonic decay widths, $\Gamma\ (V \to e^+\ e^-)$.

According to the Generalized Vector Meson Dominance Model (GVMD), the scattering amplitude for the process $\gamma + A \to B$ is the sum over the corresponding vector meson scattering amplitudes,

$$A_{\gamma+A\to B}(s,t) = \sum_V C_V A_{V+A\to B}(s,t). \qquad 14.$$

For elastic scattering, $\gamma + A \to V + A$, the cross-terms, i.e., $V' + A \to V + A$, are usually small (67) and are often neglected. The cross section is then

$$\frac{d\sigma(\gamma + A \to V + A)}{dt} = C_V^2 \frac{d\sigma(V + A \to V + A)}{dt}, \qquad 15.$$

where t is the momentum transfer from the target nucleus squared and $d\sigma/dt = |A|^2$.

The momentum transfer of the elastic scattering is determined by a hadronic form factor, $F(t)$,

$$\frac{d\sigma}{dt} = \left.\frac{d\sigma}{dt}\right|_{t=0} |F(t)|^2. \qquad 16.$$

For proton targets, the form factor is well represented by an exponential function, $|F(t)|^2 = \exp(-b|t|)$ with a slope $b \approx 10\ \mathrm{GeV}^{-2}\ \mathrm{c}^2$ for the light vector mesons (ρ, ω) and $b \approx 4\ \mathrm{GeV}^{-2}\ c^2$ for the J/Ψ. The form factor for nuclear targets is peaked at much smaller momentum transfers because of the larger size of the target.

The form factor reflects the size and shape of the target. It can, in principle, be calculated if the spatial distribution is known. The dynamical information is contained in the forward scattering amplitude, $d\sigma/dt(t = 0)$. The optical theorem relates this to the total vector meson cross section, $\sigma_{tot}(VA)$:

$$\left.\frac{d\sigma}{dt}\right|_{t=0} = C_V^2 \frac{\sigma_{tot}^2(VA)}{16\pi\hbar^2}(1 + \eta^2) \qquad 17.$$

Here, η is the ratio of the real to the imaginary part of the scattering amplitude.

In Reference (68), data on vector meson photoproduction with proton targets were used to extract the total vector meson nucleon cross section, $\sigma_{tot}(VN)$. This result was then used to calculate the total vector meson nucleus cross section, $\sigma_{tot}(VA)$, from the nuclear geometry. This gave the vector meson production cross sections for heavy-ion interactions at RHIC and the LHC shown in Table 2. For heavier vector mesons, like the J/ψ, gluon shadowing may reduce the cross section (69).

In the Glauber Model (70), the elastic scattering amplitude is given by the two-dimensional Fourier transform of the nuclear profile function, $\Gamma(b)$:

$$\frac{d\sigma(\gamma + A \to V + A)}{dt} = \frac{\pi}{\hbar^2}\left|\int e^{i\mathbf{p}_T\cdot\mathbf{b}/\hbar}\Gamma(\mathbf{b})d^2\mathrm{b}\right|^2 \qquad 18.$$

TABLE 2 Cross sections for exclusive vector meson production in Au+Au and Pb+Pb interactions at RHIC and the LHC, respectively (68)

Meson	Au+Au, RHIC σ [mb]	Pb+Pb, LHC σ [mb]
ρ^0	590	5200
ω	59	490
ϕ	39	460
J/Ψ	0.29	32

$\Gamma(\mathrm{b})$ is a function of the distribution of matter inside the nucleus, $\rho(\mathrm{b}, z)$, and the vector meson-nucleon forward scattering amplitude, f_{VN} (which can be related to the total vector meson-nucleon cross section through Equation 17):

$$\Gamma(\mathrm{b}) = 1 - \exp\left[\frac{2i\pi\hbar c}{\omega}\int \rho(\mathrm{b}, z')f_{VN}(0)\,dz'\right]. \qquad 19.$$

This approach only works for high photon energies, when $c\gamma\beta\Delta t > R_A$ so the interaction is longitudinally coherent over the entire nucleus. At lower ω, the loss of coherence reduces the cross section. The Glauber model is discussed in References (71, 72).

A Glauber model calculation of the coherent ρ^0 production cross section in Au+Au collisions at RHIC gave a total cross section of 934 mb (73). This is about 50% higher than the result in Reference (68) (cf. Table 2). The main reason for the difference is that in Reference (68), the total vector meson-nucleus cross section was calculated assuming that $\sigma_{tot}(\rho A) \approx \sigma_{inel}(\rho A)$. The calculation in Reference (73) furthermore includes the contribution from off-diagonal elements corresponding to $\rho' + \mathrm{Au} \rightarrow \rho + \mathrm{Au}$ scattering, as well as a non-zero real part of the forward scattering amplitudes (η in Equation 17). For a discussion of the $\rho' + A \rightarrow \rho + A$ contribution, see also Reference (67).

The measured ρ^0 production cross section at RHIC is $\sigma(\mathrm{Au} + \mathrm{Au} \rightarrow \mathrm{Au} + \mathrm{Au} + \rho^0) = 460 \pm 220 \pm 110$ mb at 130 A GeV (25). This can be compared with the Glauber Model calculations, which give $\sigma = 490$ mb at this energy (74). The corresponding number from the method used in Reference (68) is $\sigma = 350$ mb.

The rapidity distribution for coherent ρ^0 production measured by the STAR collaboration in Au+Au interactions at 200 A GeV is shown in Figure 4*a* (75). This is for ρ^0 production in coincidence with mutual Coulomb breakup of the beam nuclei (cf. Section 5). The rapidity distribution and cross section are in excellent agreement with the distribution obtained from the Monte Carlo model based on the calculations in Reference (76), corrected for the experimental acceptance. The reconstructed invariant $\pi^+\pi^-$ mass is shown in Figure 4*b*. The shape is well described by the sum of a relativistic Breit-Wigner function and a Söding interference term for direct $\pi^+\pi^-$ production (77). The STAR collaboration has very recently presented the first preliminary data on ρ^0 production in deuteron-gold

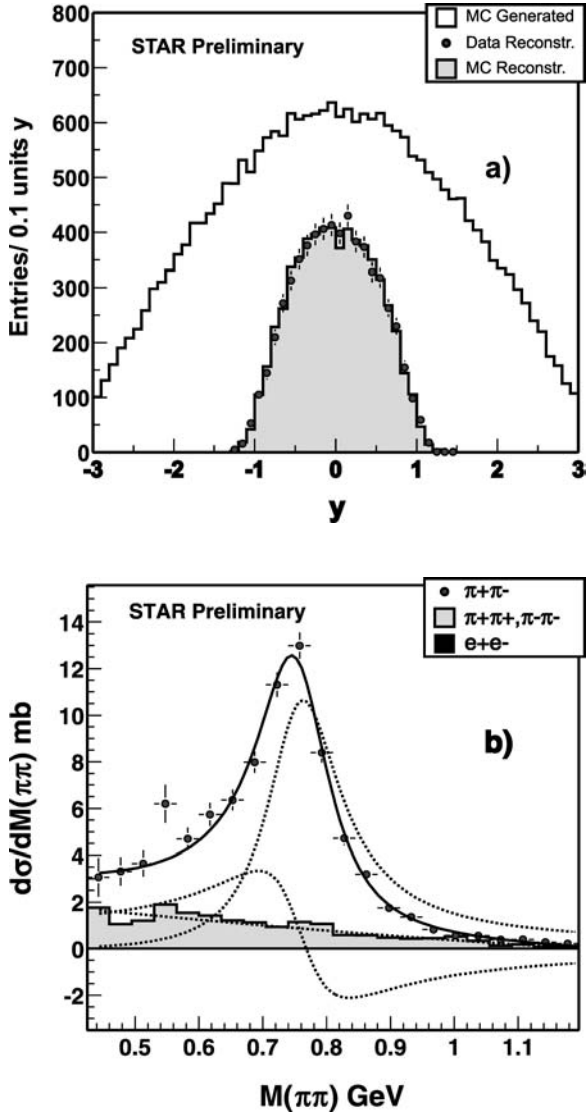

Figure 4 Rapidity (*a*) and invariant mass (*b*) distributions for coherent ρ^0 production in Au+Au interactions accompanied by mutual Coulomb breakup at $\sqrt{s} = 200$ A GeV, by the STAR collaboration. The dashed curves in (*b*) correspond to a relativistic Breit-Wigner function and a Söding interference term; the solid curve is the sum of the two. The dash-dotted curve describes the background from incoherent interactions (75).

interactions (the gold nucleus acts as photon emitter) (78) and on coherent production of $\pi^+\pi^-\pi^+\pi^-$ (79); the latter may be attributed to ρ^* photoproduction. PHENIX has shown indications of coherent J/Ψ and e^+e^--pair production in Au+Au interactions at RHIC (60, 80).

The forward scattering amplitude for heavy vector mesons has been calculated from two-gluon exchange in QCD. To leading-order (81) it was found that

$$\left.\frac{d\sigma(\gamma p \to Vp)}{dt}\right|_{t=0} = \frac{\alpha_s^2 \hbar^2 \Gamma_{ee}}{3\alpha M_V^5 c^6} 16\pi^3 \left[xg\left(x, M_V^2/4\right)\right]^2. \qquad 20.$$

Here, x is the fraction of the proton or nucleon momentum carried by the gluons, and the gluon distribution, $g(x, Q^2)$, is evaluated at a momentum transfer $Q^2 = (M_V/2)^2$. This approach has been developed further by including relativistic wave functions and off-diagonal parton distributions (82, 83). The result is a total vector meson nucleon cross section which grows rapidly with increasing photon-proton center-of-mass energy, $W_{\gamma p}$. For Υ production, $\sigma \propto W_{\gamma p}^{1.7}$ is expected.

The dependence of $d\sigma/dt$ on $[g(x)]^2$ makes exclusive vector meson production a very sensitive probe of the proton and nuclear gluon distributions. An Υ-meson produced at mid-rapidity at the LHC would come from gluons with $x \approx 7 \cdot 10^{-4}$ and $x \approx 2 \cdot 10^{-3}$ in p+p and Pb+Pb interactions, respectively.

Figure 5 shows the predicted $d\sigma/dy$ for heavy vector mesons in nucleus-nucleus and proton-proton collisions. The calculations are based on parameterizations of

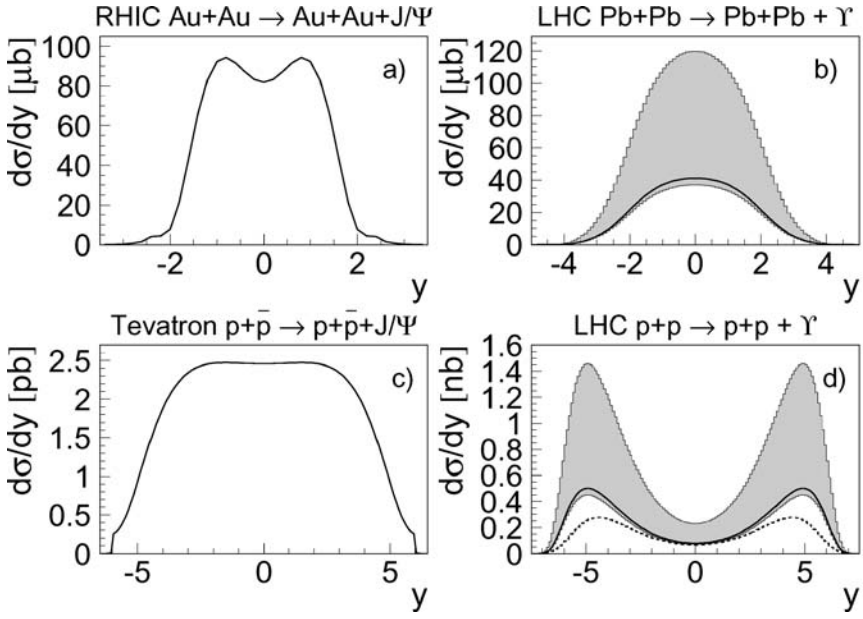

Figure 5 Rapidity distributions for exclusive J/ψ and Υ production in nucleus-nucleus and proton-proton collisions. Adapted from (21) and (68).

the photon-proton cross sections derived from measurements at HERA and from QCD-based models (21, 68). The photoproduction cross sections rise rapidly with energy. With lead at the LHC, the ρ^0 cross section is comparable to the hadronic cross section. With calcium beams at full luminosity, the LHC will produce about 230,000 ρ^0, 15,000 ϕ and 800 J/ψ per second. These rates are comparable to dedicated e^+e^- colliders, qualifying the LHC as a meson factory!

3.2. Interference in Exclusive Vector Meson Production

When a single vector meson is produced through a coherent photonuclear interaction in a nucleus-nucleus or proton-(anti-)proton collision, it is in general not possible to determine which projectile acted as target and which was the photon-emitter. The two possibilities are indistinguishable, and under certain conditions they will interfere quantum mechanically (84). Because of this interference, it is incorrect to add the cross sections for the two possibilities.

The cross section is given by adding the corresponding amplitudes A_1 and A_2

$$\frac{\hbar d\sigma}{dydp_T} = \int_{b>2R} |A_1 \pm A_2|^2 \, d^2\mathbf{b}. \qquad 21.$$

The interference is maximal at mid-rapidity, where symmetry requires that $A_1 = A_2$. For ion-ion and proton-proton collisions, the interference is destructive because of the negative parity of the vector meson; exchanging the position of the two nuclei or the two protons is equivalent to a reflection of the spatial coordinates, i.e., a parity transformation. For $p\overline{p}$ collisions, as at the Fermilab Tevatron, exchanging the proton and antiproton involves a charge-parity (CP) transformation. Since CP is positive for vector mesons, the interference is constructive at $p\overline{p}$ colliders (21).

The amplitudes A_1 and A_2 depend on the photon flux (and thus on rapidity) and on the photonuclear cross sections. Their p_T dependence comes from the convolution of the photon p_T spectrum and the p_T from the photon-nucleus scattering. The former is given by the equivalent photon spectrum (19, 85), and the latter comes from the form factor of the target.

If the outgoing vector meson is treated as a plane wave (appropriate for a distant observer), at mid-rapidity, $A_1 = A_2$ and the square of the sum of the amplitudes is

$$|A_1 \pm A_2|^2 = 2A_0^2 \left(1 \pm \cos\left(\frac{\mathrm{p} \cdot \mathrm{b}}{\hbar}\right)\right). \qquad 22.$$

For very low momenta, $p_T \ll \hbar/\langle b\rangle$, $\cos(\mathrm{p} \cdot \mathrm{b}/\hbar) \approx 1 - (\mathrm{p} \cdot \mathrm{b}/\hbar)^2/2$ and, as $p_T \to 0$, the interference is complete; emission disappears in ion-ion collisions, but doubles for $p\overline{p}$ colliders. Interference is significant for $p_T < 20$ MeV/c for the ρ^0 at RHIC (84), and $p_T < 250$ MeV/c for the J/ψ at the Tevatron (21). When $b \gg \hbar/p_T$, the cosine term oscillates rapidly as b varies, and the interference disappears. In this regime, the cross section reduces to the sum of cross sections for the two photon directions.

Away from mid-rapidity, $|A_1| \neq |A_2|$ because the photon energies for the two possibilities are different: $\omega_{1,2} = (M_V c^2/2)\exp(\pm y)$. Both the photon flux and photonuclear cross sections will be different. The interference will thus be reduced. A_1 and A_2 could also have slightly different phases, adding a phase factor δ to the cosine term in Equation 22. However, $\delta = 0$ in the standard Pomeron models (84), and a significant phase difference seems unlikely.

The interference in exclusive vector meson production is of particular interest because the vector mesons have very short lifetimes compared to the typical impact parameters. The median impact parameter for ρ^0 production in Au+Au collisions at RHIC, for example, is 46 fm, much larger than the lifetime of the ρ^0 ($\tau =$ 1.3 fm/c). The vector meson cannot, on the other hand, be produced more than $\sim$1 fm away from one of the two nuclei because of the short range of the nuclear force. Observing the expected interference pattern would thus prove that the wave function of the vector meson is preserved long after it has decayed. This is an example of the Einstein-Podolsky-Rosen paradox (84).

Preliminary data from the STAR collaboration on ρ^0 production in Au+Au at $\sqrt{s_{nn}} = 200$ GeV seem to confirm the presence of interference (86). The measured t spectrum is shown in Figure 6. The data are for interactions where both gold nuclei Coulomb dissociate. The coincident Coulomb dissociation selects events with smaller impact parameters compared to exclusive production (cf. Section 5); with Coulomb dissociation, the median impact parameter is only 18 fm (76).

The data are fit to a function,

$$\frac{dN}{dt} = a\exp(-b|t|)\,[1 + c(R(t) - 1)], \qquad 23.$$

with three parameters. These correspond to a normalization constant (a), the width of the nuclear form factor ($b \approx {R_\mathrm{A}}^2/\hbar^2$), and a parameter to quantify the magnitude of the interference (c). The function $R(t)$ is the ratio of the $d\sigma/dt$ from the Monte Carlo calculated with and without interference. This functional form separates the interference from the nuclear form factor. No interference would correspond to $c = 0$, while complete interference according to the calculations above would correspond to $c = 1$. A fit to the data finds $c = 1.01 \pm 0.08$ ($0.1 \leq y \leq 0.5$) and $c = 0.78 \pm 0.13$ ($0.5 \leq y \leq 1.0$) for the two ranges in rapidity.

3.3. Inclusive Photoproduction

The high photon flux at hadron colliders and the large total photon-hadron cross sections lead to high rates for photonuclear interactions. In Au+Au collisions at RHIC, the total photonuclear cross section for photon-nucleon center-of-mass energies above 4 GeV is about 2 barns, or nearly 1/3 of the total hadronic Au+Au cross section. The majority of these interactions are resolved interactions, i.e., they are preceded by a fluctuation of the photon to a $q\overline{q}$ state. They therefore

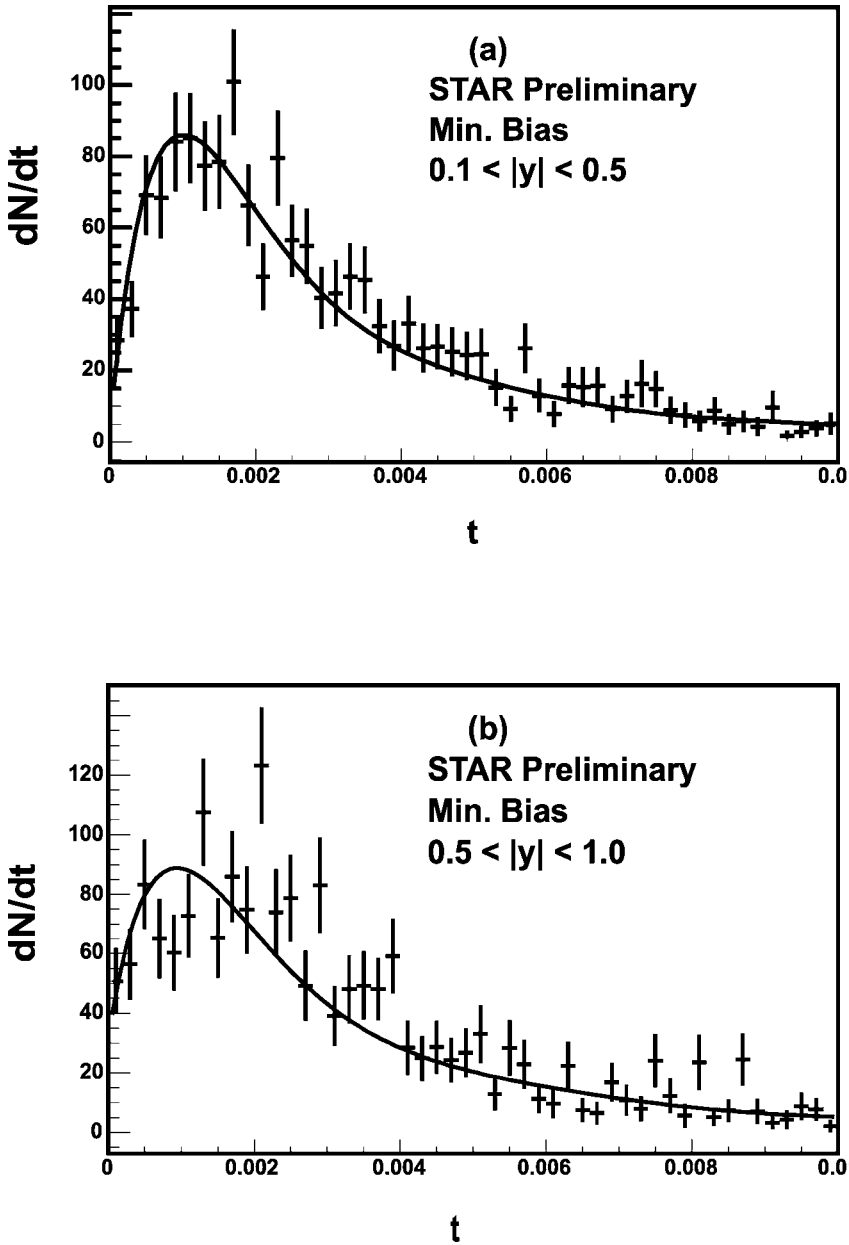

Figure 6 Efficiency corrected $t_\perp$ spectrum $t_\perp = p_{T^2}$ for ρ^0 production in Au+Au collisions at RHIC with Coulomb breakup. The points are the data, and the solid curve is a fit to Equation 23. Interference causes the dip at low $t \leq 0.001$ (GeV/c)^2 (86).

resemble inelastic hadron-nucleon/nucleus collisions. Because the photon energies are much lower than the beam energies, the kinematics is similar to that of fixed target interactions.

Despite the large cross section, particle production in resolved photon-nucleon/nucleus interactions at hadron colliders has so far attracted relatively little interest. See, however, Reference (87). Understanding the kinematics of these interactions is nevertheless essential, because they are a significant background to other ultra-peripheral processes, particularly at the trigger level (88).

Considerably more interest has been devoted to direct photon interactions, in particular the production of heavy $q\overline{q}$-pairs (6, 89–91). Recently, the cross section for photoproduction of heavy quark pairs in pp collisions has been calculated (92). In these interactions, a photon interacts with a parton in the target and the partonic cross section can be calculated from QCD.

The leading order contribution to the photoproduction of a $q\overline{q}$-pair corresponds to photon-gluon fusion, as is illustrated in the Feynman diagram in Figure 1*d*. The cross section for the partonic sub-process is (93, 94)

$$\sigma_{\gamma g\to q\overline{q}}(W_{\gamma g}) = \frac{\pi e_q^2 \alpha_{em}\alpha_s(Q^2)\ \hbar^2 c^2}{W_{\gamma g}^2}\left[(3-\beta^4)\ln\left(\frac{1+\beta}{1-\beta}\right) - 2\beta(2-\beta^2)\right]. \quad 24.$$

Here, m_q and e_q are the quark mass and electric charge, respectively, $\beta = (1 - 4m_q^2c^4/W_{\gamma g}^2)$ and $W_{\gamma g}$ is the photon-gluon center-of-mass energy. If the gluon carries a fraction x of the nucleon momentum, then $W_{\gamma g}^2 = 2\omega x\sqrt{s}$. The strong coupling constant, $\alpha_s(Q^2)$, is evaluated to one loop at scale $Q^2 = m_q^2c^2 + p_T^2$, where p_T is the quark transverse momentum.

The total photoproduction cross section $\sigma(A[\gamma]A \to Aq\overline{q}X)$ is obtained by convoluting the partonic cross section with the equivalent photon flux, $n(\omega)$, and the nuclear/nucleon gluon distribution, $G^A(x_2, Q^2)$, i.e.,

$$\sigma(A[\gamma]A \to Aq\overline{q}X) = \int\int \frac{n(\omega)}{\omega} G^A(x, Q^2)\sigma_{\gamma g}(W_{\gamma g})\,\Theta\left(W_{\gamma g} - 2m_qc^2\right) d\omega\, dx. \quad 25.$$

This equation is the equivalent of Equation 2 for two-photon interactions with the photon flux from one nucleus replaced by the gluon distribution, $G^A(x, Q^2)$. The final state $q\overline{q}$ rapidity depends on the photon energy and the gluon x. The rapidity distributions of bottom and top quarks produced in Pb+Pb and O+O collisions at the LHC are shown in Figure 7. The kinematics are discussed in more detail elsewhere (91, 95). The $q\overline{q}$ production cross section is peaked near threshold, $W_{\gamma g} \approx 4m_q^2$. Mid-rapidity production of $c\overline{c}$- and $b\overline{b}$-pairs therefore mainly probes x-values of $x \sim 1 \cdot 10^{-3}$ ($c\overline{c}$) and $x \sim 3 \cdot 10^{-3}$ ($b\overline{b}$) in heavy-ion collisions at the LHC. The corresponding numbers at RHIC are $x \sim 2 \cdot 10^{-2}$ and $x \sim 1 \cdot 10^{-1}$. (For a $q\overline{q}$-pair with invariant mass $W_{\gamma g}$ and pair-rapidity y, $x = (W_{\gamma g}/\sqrt{s})e^y$.)

The total cross sections for $c\overline{c}$ and $b\overline{b}$ production in various systems at RHIC and the LHC are listed in Table 3. The calculations without shadowing are compared

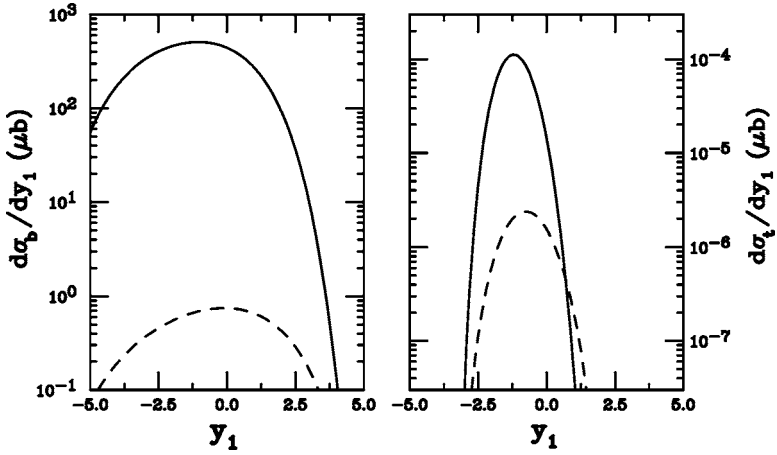

Figure 7 Rapidity distributions of (*left*) and (*right*) quarks produced in photonuclear collisions at the LHC. The solid and dashed curves are for Pb+Pb and O+O interactions, respectively. Here, the photon is emitted by the nucleus with positive rapidity; the complete cross section is the sum of this curve plus its mirror image. Shadowing is included using the parameterizations of Reference (62). Adapted from References (90, 91).

with two calculations that include nuclear modifications. As expected, shadowing has the largest effect on the production of lighter quarks ($c\overline{c}$) using heavy nuclei. The cross section for producing a $c\overline{c}$-pair in Pb+Pb interactions at the LHC is of the order of 1 b, nearly 1/6 of the total hadronic cross section.

Quark pairs can also be produced in anomalous interactions, where a parton from the resolved photon interacts with a parton in the target, or in two-photon interactions. The contribution from these processes is small compared with the direct production cross section (91). The anomalous cross sections are 1–20% of the direct cross sections, depending on quark flavor and collision energy. The two-photon contribution is usually less than 1% of the anomalous cross section.

In addition to probing the nuclear gluon distribution, photon-gluon fusion reactions are of interest as a means to determine the electric charge of the top quark. The top quark measurements are all consistent with a standard model top with electric charge $q_t = +2/3$. However, since the correlation between the decay products $W^+ \leftrightarrow b$ or $W^- \leftrightarrow \overline{b}$ are never measured, q_t is unconstrained (96). The data can still accommodate an exotic particle t' with $q_t = 4/3$, which decays via $t' \rightarrow W^- + b$. Because the cross section for $\gamma + g \rightarrow q + \overline{q}$ is proportional to q_t^2, $q_t = -4/3$ would quadruple the cross section.

There have so far been no experimental measurements of heavy quark pair photoproduction in heavy-ion or pp collisions. Some of the experimental techniques

TABLE 3 Cross sections for $q\overline{q}$ photoproduction through direct photon-gluon fusion in heavy-ion interactions. The numbers in columns 4 and 5 include nuclear gluon shadowing from References (62) and (97), respectively.

	$q\overline{q}$ **cross sections in heavy-ion collisions**			
Colliding system	**Flavor**	σ **[mb] No shadowing**	σ **[mb] EKS98**	σ **[mb] FGS**
RHIC Au+Au	$c\overline{c}$	15.8	17.4	17.6
RHIC Au+Au	$b\overline{b}$	$2.9 \cdot 10^{-3}$	$3.0 \cdot 10^{-3}$	$3.0 \cdot 10^{-3}$
RHIC Si+Si	$c\overline{c}$	0.196	0.203	0.20
RHIC Si+Si	$b\overline{b}$	$1.07 \cdot 10^{-4}$	$1.13 \cdot 10^{-4}$	$1.14 \cdot 10^{-4}$
LHC Pb+Pb	$c\overline{c}$	1250	1050	850
LHC Pb+Pb	$b\overline{b}$	4.9	4.7	4.4
LHC Ar+Ar	$c\overline{c}$	16.3	14.3	12.3
LHC Ar+Ar	$b\overline{b}$	0.073	0.070	0.066

that could be used to separate this signal from hadronic backgrounds are discussed in Section 6.

3.4. Dijets, Compton Scattering, Vector Boson Production and Other Processes

When the final state quarks in the process shown in Figure 1*d* have high p_T, the final state is two roughly back-to-back jets (98). The cross section is calculated in a manner similar to that of Equation 24, except that light quarks are included. Jets may also be produced to leading order through the process $\gamma + q \rightarrow g + q$. The cross section for dijet production is sensitive to the gluon distribution in the target; because of the simplicity of the reaction, there are fewer systematic uncertainties than in other processes such as vector meson production. However, it may be more difficult to isolate dijet photoproduction from backgrounds such as hadronic production of dijets and diffractive hadronic production.

Since the gluon-contributing nucleus does not stay intact, the experimental signature for this process is two jets, accompanied by a single rapidity gap between the jets and the photon-emitting nucleus. The two jets may have very different rapidities and it may be difficult to reconstruct the entire event. Calculations have considered the case where a single jet is detected, with $|\eta| < 1$ (98). Without shadowing, the rate to photoproduce jets with energies above 21 GeV in lead-lead collisions at the LHC is 0.015 Hz. In a 10^6 s run, jets up to 80 GeV should be detectable.

A closely related process is the production of a photon + jet final state; this is essentially Compton scattering. The rates for this process are about two orders of magnitude below that for dijet production (98).

The strong Coulomb fields may also dissociate hadrons into jets. For example, a proton may fragment into three quarks, leading to a reaction such as $\gamma p \rightarrow 3$ jets; this would be a distinctive signature in pA collisions (99). One photon can also dissociate another, leading to reactions such as $\gamma\gamma \rightarrow 2$ jets (99, 100).

$W^{\pm}$ and Z^0 can be photoproduced in ultra-peripheral collisions. A Z^0 can be produced when a photon fluctuates to a $q\overline{q}$ pair, scatters from a target nucleus and emerges as a Z^0. In the high-energy limit, the cross section for $\gamma p \rightarrow Z^0 p$ is about 0.01 pb (101). Unfortunately, even with a coherent photon beam, the cross section seems too low to be observable.

$W^{\pm}$ pairs can be produced directly from a photon fluctuation, $\gamma \rightarrow W^+W^-$. One of the Ws can interact with the target nucleus, leading to a hadronic jet plus a real W. Unfortunately, this process has not been studied in detail.

4. TWO-PHOTON PROCESSES

4.1. Production of Free- and Bound-Pairs

Between 1933 and 1937, Furry, Carlson, Landau, Lifshitz, Bhabha, Racah, Nishina, Tomonaga, and several others performed calculations of e^+e^- production in relativistic collisions of fast particles (cosmic rays) (102–106). The purpose was to test the newly born Dirac theory for the positron. Starting with the Dirac equation for the electron and its antiparticle, they found (106),

$$\sigma = \frac{28}{27\pi}\sigma_0[L^3 - 2.198L^2 + 3.821L - 1.632], \qquad 26.$$

where $\sigma_0 = (Z_1 Z_2 \alpha^2 \hbar / m_e c)^2$, $L = \ln(\gamma_1\gamma_2)$, and γ_i is the Lorentz factor of ion i in the laboratory system. The first term of this equation can be simply obtained from Equation 1 and the cross sections for $\gamma\gamma$ pair production. The production cross sections for heavy lepton pairs ($\mu^+\mu^-$, or $\tau^+\tau^-$) can be obtained similarly. The production of $\mu^+\mu^-$ pairs using hadron beams was first observed in 63 GeV pp collisions at CERNs Intersecting Storage Rings (107).

For meson pairs like $\pi\pi$, neglecting internal substructure, as is done for Equation 26, may be appropriate near threshold. However, at higher pair masses, the quark substructure of the mesons becomes important, and the cross section for $\gamma\gamma \rightarrow \pi^0\pi^0$ becomes comparable to that for $\pi^+\pi^-$ (108). In fact, studies of $\gamma\gamma$ production of mesons pairs are interesting probes of meson structure. Baryon-antibaryon pairs are also of interest, because the cross section is sensitive to the baryon internal structure.

Because the cross sections depend on the inverse of the square of the particle mass, production of heavier pairs ($\mu^+\mu^-$, $\tau^+\tau^-$) is much smaller than for e^+e^-. Their Compton wavelength, $\lambda_i = \hbar/m_i c$, is smaller than the nuclear radius R. This requires the replacement $L \rightarrow \mathcal{L} = \ln(\gamma_1\gamma_2\delta/m_i c R)$ in Equation 26, where $\delta = 0.681\ldots$ is a number related to Euler's constant.

Bound particles, such as positronium or $q\overline{q}$ mesons, are also produced in two-photon interactions. The cross section is given by Equation 2. The cross section for $\gamma_1\gamma_2 \to X$ depends on the particle's decay width to two photons, $\Gamma_{\gamma\gamma}$ (109). Because decay and $\gamma\gamma$ production use the same matrix elements, only the phase-space factors and polarization summations are distinct. One finds (109)

$$\sigma(\omega_1, \omega_2) = 8\pi^2(2J+1)\frac{\Gamma_{\gamma\gamma}}{Mc^2}\,\delta\left(4\omega_1\omega_2 - M^2c^4\right) \qquad 27.$$

where J, M, and $\Gamma_{M\to\gamma\gamma}$ are the spin, mass, and two-photon decay width of the meson, respectively. The delta-function imposes energy conservation.

Using Equation 27, the production of mesons with mass M in HI colliders is (9):

$$\sigma = \frac{128}{3}(Z_1Z_2\alpha)^2\,\frac{\hbar\Gamma_{\gamma\gamma}}{M^3c^5}[\mathcal{L}^3 + \cdots]. \qquad 28.$$

This equation is obtained using Equation 2 and the high-energy limit ($\gamma \gg 1$) of the equivalent photon number $n(\omega)$ (for more details, see Reference (110)).

A more detailed account of the space geometry of the two-photon collision is necessary (18) and will be discussed in Section 4.4. Because spin 1 particles cannot couple to two real photons (111), only spin 0 and spin 2 particles should be produced.

The treatment of bound states in quantum field theory (QFT) is a very complex subject (for reviews, see References (112, 113)). In the case of positronium production by two photons (para-positronium) and by three photons (ortho-positronium), standard QFT techniques allow a simple and accurate way to calculate the cross sections from first principles (114, 115). The para-positronium production cross sections are quite large, 19.4 mb and 116 mb, for RHIC (Au+Au) and LHC (Pb+Pb), respectively (115). However, Coulomb corrections reduce these values by as much as 43% for RHIC and 27% for LHC (114). The cross sections for the production of ortho-positronium, which requires three-photon exchange, are also large: 11.2 mb and 35 mb, for RHIC and LHC, respectively (114). Even the ortho-positronium cross sections correspond to production rates of 4 and 35 per second respectively. If the positronium could be extracted from the interaction points, they could be used to test interesting properties of QFT for bound states. Relativistic positronium has an unusually large transparency in thin layers (see Reference (116) and references therein).

The same diagrams for the calculation of the positronium apply for production of bound $q\bar{q}$ pairs (mesons) in UPC (115). However, proper accounting for the color degrees of freedom is needed (117).

4.2. Production of Free e^+e^- Pairs

Due to experimental difficulties, Equation 26 (and its newer counterparts) has never been fully tested. With the construction of RHIC and the LHC, interest in this process has grown. For heavy ions, the e^+e^- production probabilities are

close to one, and lowest-order perturbative calculations of the cross sections violate unitarity (i.e., $d^2\sigma/d^2b > 1$) (9).

This observation led to more detailed calculations (19, 118–122), involving high-order processes, such as the exchange of multiple photons (Coulomb distortion) and the production of multiple pairs, as shown in Figures 1*e*, *f*. These processes are important for collisions at small impact parameters. Diverse theoretical methods have been considered. Perturbative calculations are simple to write down, but they involve rather complicated integrals, especially for low-energy electrons, due to Coulomb distortion and relativistic effects on the continuum electronic wavefunction (9). A general sum of the contribution of diagrams like those in Figure 1*e*, *f* and unitarity corrections (involving the production of virtual e^+e^- pairs) was obtained in Reference (123). To account for Coulomb distortions, one needs to add to Equation 26 a term of the form [see eq. 7.3.10 of Reference (9)],

$$\sigma_C = -\frac{28}{9\pi}\left[f(Z_1\alpha) + f(Z_2\alpha)\right]\sigma_0 L^2, \qquad 29.$$

where

$$f(x) = x^2 \sum_{n=1}^{\infty} \frac{1}{n(n^2 + x^2)} \qquad 30.$$

is the Bethe-Maximon correction. Equation 29 has been correctly derived in Reference (124). Their result was later confirmed by independent calculations in Reference (125). For Pb+Pb collisions at LHC, the Coulomb distortion correction reduces the pair-production cross section by 14%. Other unitarity corrections further reduce the cross sections by 3% (123).

The calculation of the production of multiple pairs, as shown in Figure 1*e*, *f*, is directly connected with the unitarity problem. It is possible to interpret $d^2\sigma/d^2b$ as the mean number of pairs produced at a given impact parameter. For Ca-Ca collisions at the LHC ($Z\alpha = 0.15$), $\sigma_{2-pairs} = 0.11$ b (123), or about 27,000 $e^+e^-e^+e^-$ events per second. In the literature one finds different methods to calculate the cross section for the production of $n > 2$ pairs. Reference (123) does a simple fit to numerical calculations. Reference (117) is based on the expression for the probability $P(b)$ of the pair production taken from Reference (9). Reference (122) claims that this expression is wrong. They derived expressions for this probability using two different methods. Reference (123) obtains $\sigma_n \propto L^n$, whereas References (118) and (124) obtain $\sigma_n \propto L^{2n}$ and $\sigma_n \propto L^{3n}$, respectively. The calculations differ in the method used to include Coulomb and unitarity corrections. The production of multiple pairs has been studied with a variety of different theoretical approaches (14, 123, 125, 127, 133–137).

The calculation of multiple photon exchange can be considerably simplified in the ultra-relativistic limit. In this limit, the electromagnetic field of the ions is squeezed in the plane perpendicular to its trajectory (i.e., it can be approximated by a delta-function along this plane). In the appropriate gauge, the Coulomb

potential is two-dimensional and the time-dependent Dirac equation may be solved exactly (130, 138, 139). This should be equivalent to an all-orders perturbative calculation.

This approach yields good results as long as $\omega b/\gamma\hbar c \leq 0.1$ (140). Above this value, the delta-function approximation breaks down. Because the most important impact parameters for this process are of order $b \simeq \hbar/m_e c$ (9), the calculation can be separated into two regions: (a) $b \simeq \hbar/m_e c$ where the approximation is valid; and (b) large impact parameters, for which perturbative calculations are accurate (130, 138, 139). This method describes well the differential cross sections for e^+e^- pair production up to energies of order 0.1 $\gamma m_e c^2$, above which the delta-function approximation breaks down for the same reason as above (140). The initial calculations using this technique found results that matched the lowest order perturbation theory without Coulomb corrections (131, 132). This was inconsistent with both theoretical expectations and with data (132). However, regularization of the integrals was critical; with this regularization, the Dirac approach reproduced the lowest order result, with Coulomb corrections (126, 141). This technique allows for the calculation of cross section for free e^+e^- pair production to all orders in $Z\alpha$ (141).

Electron-positron pair production has been studied at RHIC in combination with mutual Coulomb excitation (142). As will be discussed in the next section, the mutual Coulomb excitations were required to trigger on these events, and also had the effect of selecting events with $b < 30$ fm, where non-perturbative effects were strongest. The cross section, pair mass, rapidity and pair p_T distributions were all in accord with the predictions of lowest order perturbation theory (136). The pair p_T distribution deviated from the Weiszaecker-Williams virtual photon approach, showing that the photon mass was important in that kinematic regime.

The STAR study suffered from low statistics. Earlier experiments on e^+e^- production in sulfur-platinum (and sulfur-nuclei) collisions at the CERN SPS had higher statistics, but lower beam energies; they also found good agreement with lowest order calculations (143, 144).

It remains disappointing that these 70-year-old QED calculations are still not fully tested. Although many aspects of QED have been tested to high precision, studies involving strong fields are much less advanced; pair production with relativistic heavy ions (with $Z\alpha \sim 1$) is one important example.

4.3. Pair Production with Capture and Antihydrogen

An important phenomenon occurs when the electron is captured in an atomic orbit of the projectile or of the target (9). At RHIC and the LHC, this is an important source of beam particle loss (110). The produced beam of single-electron ions carries considerable power (145); at the LHC, at full luminosity, the produced $^{+81}$Pb beam carries sufficient power to quench the superconducting accelerator magnets; this limits the LHC luminosity with heavy ions (146).

One striking application of this process was the recent production of antihydrogen atoms using relativistic antiproton beams (7). Here the positron is produced and captured in an orbit of the antiproton. The expression

$$\sigma = 3.3\pi \frac{Z_1^2 Z_2^6 \alpha^8 \hbar^2}{m_e^2} \frac{1}{\exp(2\pi Z_2 \alpha) - 1} (L - 2.051) \qquad 31.$$

for pair production with electron capture in the nucleus with charge Z_2 is obtained in first order perturbation theory (9). Although Equation 31 works reasonably well for explaining antihydrogen production, it is only valid for small Z_i ($Z_i \leq 15$) (7, 147, 148). For large Z_i, as with the experiments at RHIC and LHC, non-perturbative calculations may be necessary (119, 130, 149–152). Equation 31 includes higher order effects related to the electron capture, but is not a complete all-orders result. The additional higher order corrections are apparently small, and Equation 31 should be usable for most purposes. The fraction with the exponential term is due to the distortion of the positron wavefunction. It accounts for the reduction of the magnitude of the positron (continuum) wavefunction near the nucleus where the electron is localized (bound).

Equation 31 shows that the cross section depends on energy as $\sigma = A \ln \gamma_1 \gamma_2 + B$, where the coefficients A and B depend on the nuclear charges. This scaling was confirmed in numerical calculations of Reference (130) and was used in the analysis of the experiment in Reference (153), shown in Figure 8*a*. The comparison between theory and the data of Reference (153) is not completely

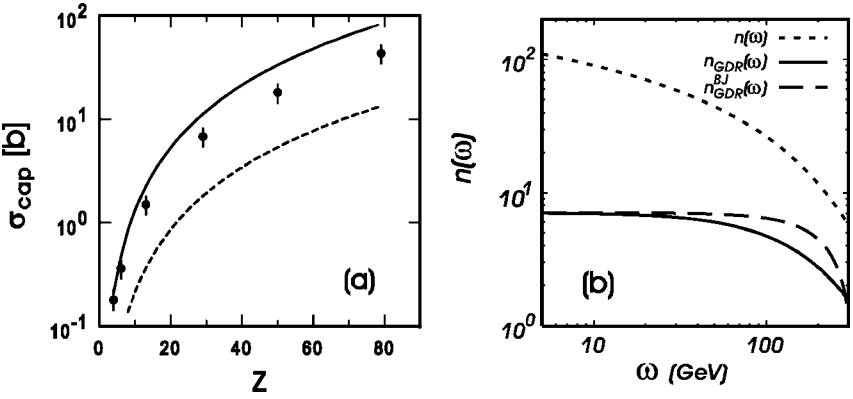

Figure 8 (*a*) Pair production with capture for Pb^{82+} (33 TeV) beams on several targets. The solid and dashed curves are theoretical calculations (153). See text for more details. (*b*) The tagged total photon flux (accompanied by a single giant dipole resonance excitation) for a complete calculation (*solid line*) and a simplified "box" integration (*dashed line*), compared to the untagged flux (*dotted line*), for gold at RHIC. Although tagging reduces the low-energy flux by an order of magnitude, at high energies, the difference is much smaller. From Reference (22).

valid because atomic screening was not included. When screening is present, the cross sections are smaller by at least a factor of 2-4 (see Equation 7.4.3 of Reference (9)).

Similar reactions occur with hadron pairs. Processes like pion pair production with capture (or, similarly, photoexcitation of a Δ resonance, which decays by π^+ emission) increase the nuclear charge by 1 and can turn lead into bismuth, plus a π^+. This change cannot occur electromagnetically, because e^+ will not bind to lead. These transmutations have been studied at the SPS/CERN for ^{208}Pb at 160 GeV/nucleon (154). The data can be described quantitatively with electromagnetic excitation calculations (87, 155). For high-Z nuclei, the dominant contribution to nuclear-charge pickup is due to electromagnetic production of π^- by virtual photons. This contribution is completely negligible for a similar experiment at an energy of 10.6 GeV per nucleon (156).

4.4. Two-Photon Production of Mesons

For the production of composite particles, one can use Equation 28 as a first guess. However, even the lightest mesons (π^0) require photons of relatively large energy ($\geq$70 MeV). Mesons are produced primarily in collisions with relatively small impact parameters (compared to $2R_A$) where hard photons are more abundant. Substantial changes to Equation 28 are required to account for the collision geometry (18, 157).

One can rewrite Equation 2 more conveniently as

$$\sigma_X = \int ds \frac{d\mathcal{L}(W_{\gamma\gamma})}{dW_{\gamma\gamma}} \sigma_{\gamma\gamma\to X}(W_{\gamma\gamma}), \qquad 32.$$

where $W_{\gamma\gamma} = 4\omega_1\omega_2$ is the square of the center-of-mass energy of the two photons, $\sigma_{\gamma\gamma\to X}(W_{\gamma\gamma})$ is the two-photon production of particle X, and $d\mathcal{L}/dW_{\gamma\gamma}$ is the "photon-photon luminosity." $d\mathcal{L}/dW_{\gamma\gamma}$ can be multiplied by the ion beam luminosities, yielding an effective two-photon luminosity $d\mathcal{L}_{eff}/dW_{\gamma\gamma}$ which can be directly compared to other two-photon luminosities, such as at e^+e^- or pp colliders (158). With heavy-ion beams, the LHC two-photon luminosities are much higher than are available elsewhere, either with proton beams at the LHC or at the e^+e^- LEP-II collider for energies up to $\sqrt{W_{\gamma\gamma}} \approx 500$ GeV (14).

Table 4 (115) shows the cross sections for the production of $C = even$ mesons for the RHIC and LHC colliders. Other calculations were done in References (88, 100, 159). The cross section corresponds to a $\gamma\gamma \to \pi^0$ rate of 30 events/second with lead beams at the LHC. For heavier mesons, like η_c, the rate is still large, of the order of 1 per minute.

For mesons of comparable mass, the two-photon cross sections in Table 4 are about two orders of magnitude lower than the cross sections for photonuclear vector meson production (Table 2). This difference stems from the different coupling strengths of the strong and electromagnetic interactions, $\alpha_s \sim 1$ vs. $\alpha_{em} \approx 1/137$.

TABLE 4 Cross sections for two-photon production of ($C = even$) mesons at RHIC (Au+Au) and at LHC (Pb+Pb) (115)

Meson	Mass [MeV]	σ^{RHIC} [mb]	σ^{LHC} [mb]
π_0	134	4.9	28
η	547	1.0	16
η'	958	0.75	21
$f_2(1270)$	1275	0.54	22
$a_2(1320)$	1318	0.19	8.2
η_c	2981	3.3×10^{-3}	0.61
χ_{0c}	3415	0.63×10^{-3}	0.16
χ_{2c}	3556	0.59×10^{-3}	0.15

Two-photon meson spectroscopy is thus greatly complicated by the large background from photonuclear interactions. For example, with lead beams at the LHC, the rate of J/ψ photoproduction followed by $J/\psi \to \gamma\eta_c$ is about 2.5 per minute, higher than the $\gamma\gamma \to \eta_c$ rate.

Although it may be possible to separate the different event classes with cuts on meson p_T, rapidity, and final state particles, the vector meson background seems daunting to most efforts (68).

4.5. Searches for New Physics

The LHC will reach high enough energies that two-photon interactions will be an attractive place to search for some types of new physics. Many early calculations focused on the search for the Higgs particle (163–165). Other examples include supersymmetric particle pairs, magnetic monopoles, and possible extra spatial dimensions (14). The LHC will also be able to probe vector boson couplings through reactions like $\gamma\gamma \to W^+W^-$.

The two-photon production rate for the Higgs is small enough that, for most models, it is likely to be discovered in hadronic interactions. However, for standard model Higgs masses under $\approx$200 GeV, with medium ion beams, the $\gamma\gamma$ channel should produce a handful of events per year (14). In some supersymmetric scenarios, the production of the Higgs in UPCs could be significantly enhanced (159). The $\gamma\gamma$ production channel could also be studied in pp collisions; the greatly increased luminosity and running time will more than compensate for the smaller production cross section. However, in pp collisions, there is a considerable background due to diffractive interactions. It may be possible to separate $\gamma\gamma$ from diffractive interactions by studying the p_T of the scattered protons. This could be done by placing small detectors, known as Roman pots, inside the beampipe, to detect protons scattered at very small angles (160).

Supersymmetric particle pairs are a similar story. If present, they are likely to be discovered in hadronic interactions. However, if supersymmetry is correct, a large number of new particles are likely to be present, and the $\gamma\gamma$ production of sparticle pairs is likely to provide significant new information; two-photon production is sensitive to significant regions of phase space (159). Two-photon interactions are sensitive to sparticles that do not participate in the strong interaction. Photonuclear interactions may also be useful for studying supersymmetry.

Real or virtual magnetic monopoles can be produced by two-photon fusion. Investigators searched for the process $\gamma\gamma \rightarrow \gamma\gamma$ at the Fermilab Tevatron, and mass limits were set on magnetic monopoles with various charges (161). The LHC will be able to do far better.

The presence of extra dimensions could be detected via the two-photon production of gravitons. The cross section to produce a graviton, $\gamma\gamma \rightarrow G$ increases in the presence of compact dimensions (162). There are unresolved theoretical issues regarding the cross section, but one calculation finds that, for 2 extra compact dimensions, at the LHC, the cross section is of order 1 nb for lead and 10 pb for calcium (162). Rates are not given for proton beams, but for calcium, and likely protons, a few events would be produced each month. The experimental signature of graviton production has not been worked out in detail.

Most of these new physics channels involve relatively high p_T particles and so should be within the purview of the planned trigger setup for the ATLAS and CMS detectors. This may not be true for supersymmetric final states; two charged sleptons that do not interact hadronically will challenge any trigger.

5. MULTIPLE INTERACTIONS BETWEEN A SINGLE ION PAIR

Because heavy ions have such large charges, a single ion pair can undergo multiple electromagnetic reactions in a single interaction. Even though the reactions may be independent, the geometry introduces correlations between the photon energies and polarizations. Multiple interactions are also a key experimental tool, allowing for many cross checks under different triggering conditions. One example of such a reaction is the photoproduction of a ρ^0 meson, accompanied by the mutual Coulomb excitation of both nuclei:

$$\mathrm{Au} + \mathrm{Au} \rightarrow \mathrm{Au}^* + \mathrm{Au}^* + \rho^0. \qquad 33.$$

This reaction was studied by the STAR collaboration (25). This process occurs predominantly via 3-photon exchange, as is shown in Figure 1*g*.

Investigators have also observed four photon reactions, such as the production of an e^+e^- pair accompanied by mutual Coulomb excitation (142), as shown in Figure 1*h*.

In a multi-photon process, each photon emission may be treated independently if the energy lost by the nucleus is not significant. As long as the photon emission

does not excite the emitter, the reactions may be treated as completely independent. The cross section is calculated in impact parameter space

$$\sigma = \int d^2b P(b) \qquad 34.$$

where $P(b)$ is the probability for the reaction to occur at impact parameter b. This is

$$P(b) = \int \frac{d\omega}{\omega} N(\omega, b)\sigma_{\gamma A}(\omega). \qquad 35.$$

When the cross section for a reaction is very large (as with e^+e^- production or GDR excitation), the naive $P(b)$ calculated in Equation 35 may exceed 1. $P(b)$ should then not be interpreted as a probability but rather as the mean number of produced particles at that impact parameter. The actual number of produced particles follows a Poisson distribution with this mean. The generalization to 2 (or more) photon exchanges is obvious. Calculations using this approach accurately predicted the cross section and kinematic distributions for Reaction 33 (25).

This factorization only holds if several conditions are satisfied. Photon emission must not excite the emitting nucleus, and the photons must be emitted independently. As long as the fractional energy loss of the nuclei is small, this is valid (168). Finally, the excitation must not change the nuclear form factor significantly on the time scale of the reaction (the frozen nucleus approximation). As long as these strictures are satisfied, the ordering of the subprocesses is unimportant. These conditions hold for heavy-ion collisions. For proton beams, with $\eta = Z_1 Z_2 e^2\alpha/\beta < 1$, the factorization is on weaker ground because of the poorly defined impact parameter (22).

It can be convenient to treat one reaction as a trigger (or selector) for a range of impact parameters. Picking events with mutual Coulomb excitation, for example, selects events with small impact parameters. The reason can be seen in Equation 34. In the low-energy limit ($\omega \ll \gamma\hbar c/R_A$), for a fixed ω, $P(b) \approx N(\omega, b) \approx 1/b^2$. For a two-photon reaction, $P_1(b)P_2(b) \approx 1/b^4$. The mean impact parameter b_n for an n-photon interaction is (22)

$$\overline{b}_n = \frac{\int d^2b b P_1(b) \ldots P_n(b)}{\int d^2b P_1(b) \ldots P_n(b)}. \qquad 36.$$

Here, $b_{min} = 2R_A$ is the minimum impact parameter, and $b_{max} = \gamma\hbar/R_A$. For $n = 1$ the result $\overline{b} = (b_{max} - b_{min})/\ln(b_{max}/b_{min})$ is not so useful. However, for 2 or more photon exchanges

$$\overline{b}_{n>1} = 2R_A \frac{2n-2}{2n-3}; \qquad 37.$$

b_{max} drops out, leaving a simple result. For $n = 2$, this reduces to $\overline{b}_2 = 2R_A$; for larger n, $\overline{b}$ is even smaller. At heavy-ion colliders, mutual Coulomb excitation is an

effective trigger for selecting low-impact parameter events. Detailed calculations of the median impact parameter in 1 and 3 photon interactions find a similar scaling (76). Reducing $\overline{b}$ is very helpful in studying interference in vector meson production, by increasing the p_T range over which the interference is visible.

This selection can also be viewed in momentum space. In the low-energy limit, the photon flux $n(\omega)$ (Equation 5) scales as $1/\omega$. However, when an additional photon is present, the spectrum becomes much harder. The spectrum for photons that are accompanied by Coulomb excitation is:

$$n(\omega) \approx \int_{2R_A}^{\gamma\hbar c/\omega} d^2b N(\omega, b) \frac{\text{Const.}}{b^2} \approx \text{Const.} \qquad 38.$$

The extra photon line adds a $1/b^2$ weighting, and the resultant flux is independent of the photon energy.

Figure 8*b* compares the spectra with and without tagging. By selecting reactions with additional accompanying photon interactions, experimenters can tune their photon beam, hardening or softening the spectrum. This tuning allows many cross-checks. For example, in vector meson production, $y = \ln(2\omega/M_V c^2)$, and there is a two-fold ambiguity over which nucleus emitted the photon. By comparing vector meson production with and without mutual Coulomb excitation, it is possible to account for this ambiguity and find the production cross section as a function of photon energy.

The coupling is also very useful in experimental triggering. A simple reaction like multiple Coulomb excitation can be used to trigger on small-impact-parameter collisions; the remainder of the event can then be studied without experimental bias.

For two-photon final states, like e^+e^- pairs, the situation is more complex because the particles are produced outside the nuclei. However, two-photon reactions are also enhanced at small nucleus-nucleus impact parameters. The STAR collaboration used mutual Coulomb excitation to study low-mass e^+e^- pair production at RHIC, because it was not possible to trigger on the e^+e^- pair itself (142). The presence of the mutual excitation also significantly hardens the pair mass spectrum.

In multiple photonuclear interactions, the photon polarizations are collinear. Photons are linearly polarized along the electric field of the emitting nucleus. In photonuclear interactions, the electric field vector follows the impact parameter vector. When a single nucleus emits multiple photons, these photons all have the same linear polarization. When the other nucleus emits a photon, it will have the opposite polarization.

When the final states are sensitive to the photon polarization, then angular correlations will be present. In ρ^0 decay, in the plane perpendicular to the ρ^0 direction, the angle between the photon polarization vector and the π^+ (or π^-) direction is distributed following a $\cos\theta$ distribution. For the case of two independent ρ^0 decays, with uncorrelated photon polarization, the angle between

the two π^+, $\Delta\phi$ is evenly distributed between 0 and 2π. With the polarization correlation, the angular correlation is

$$N(\Delta\phi) \approx 1 + \frac{1}{2}\cos(2\Delta\phi). \quad 39.$$

A similar distribution is also expected for neutrons from giant dipole resonance decay. Correlations between neutron p_T in ρ^0 production and GDR excitation(s) should also be measurable at RHIC. In the longer term, GDR excitation neutrons could be used to tag photons according to their polarization direction, allowing for studies with polarized photons. Similar polarization should also occur for medium-energy nuclear reactions.

In addition to the correlations due to the geometry, multiple interactions may be a place to study Bose-Einstein correlations, such as in $\rho^0\rho^0$ production by two independent photonuclear interactions. When the two ρ^0 are produced on the same nucleus, the production should be bosonically enhanced (exhibit super-radiance) when the ρ have (in the nuclear target rest frame) a momentum difference $\Delta p < \hbar/R_A$.

6. EXPERIMENTAL POSSIBILITIES AND LIMITATIONS FOR ULTRA-PERIPHERAL COLLISIONS

The experimental study of electromagnetic interactions at high-energy colliders is quite new. Since the characteristics of these interactions are very different from the more common hadronic interactions, most existing and planned detector systems are not optimized to study them. This section will discuss some of the general experimental possibilities and limitations at current and future colliders.

With hadron colliders (unlike electron beams) it is generally not possible to detect the outgoing projectiles following an electromagnetic interaction. This is because of the small momentum transfers involved. Tagging of nuclei will never be possible because the angular deflection following the coherent emission of a photon is smaller than the angular dispersion of the beam. Proton tagging has been proposed, but requires extremely high resolution Roman pots (160).

For exclusive particle production, characterized by the emission of only a few final state particles, good signal to background ratios can be achieved by selecting events with small total transverse momentum when the event is reconstructed (88). The total event transverse momentum is the sum of the momentum transfer from each projectile, which is determined by the form factors and can be calculated accurately. The method works best for heavy nuclei. This is illustrated in Figure 9, which shows the p_T distribution for exclusive ρ^0 production in Au+Au interactions at RHIC. The coherent peak for events with exactly one reconstructed π^+ and one reconstructed π^- can be clearly seen with $p_T < 100$ MeV/c. The incoherent background can be estimated by measuring events with two reconstructed pions

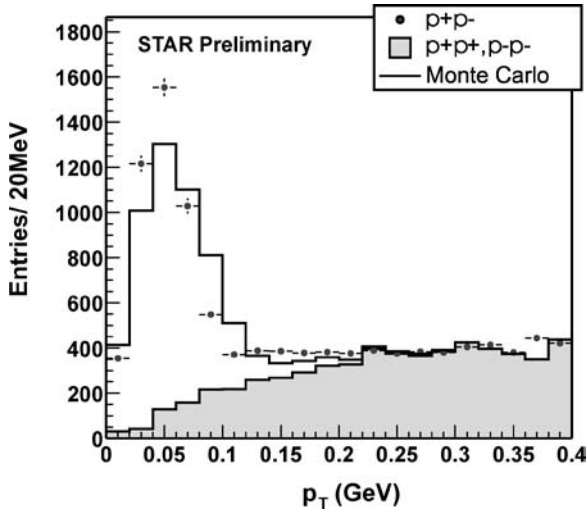

Figure 9 Transverse momentum distribution for events with exactly 2 reconstructed charged pions. Data from the STAR collaboration (75). The Monte Carlo calculation is based on Reference (76).

with the same charge (dashed histogram in the figure). The technique of using the total event p_T to identify electromagnetic interactions works only for coherent and exclusive particle production. Other photonuclear interactions require different methods. Incoherent photon-induced interactions are characterized by a gap in rapidity, void of particles, between the rapidity of the photon-emitting projectile and the rapidity of the produced state. This distinguishes the electromagnetic interactions from ordinary hadronic interactions.

In hadronic interactions, the probability of having a rapidity gap of width Δy void of particles decreases exponentially with increasing size of the interval:

$$p(n = 0) = \exp(-\langle dn/dy \rangle \Delta y) \qquad 40.$$

where $\langle dn/dy \rangle$ is the mean multiplicity per unit of rapidity. Requiring a rapidity gap of width $\Delta y = 2$ leads to a hadronic rejection factor of 10^{-2} to 10^{-3} for single nucleon-nucleon interactions at RHIC and LHC energies. Additional rejection of hadronic events can be obtained if the fragmentation of the beam nuclei is detected, for example in forward (zero-degree) calorimeters. In hadronic interactions, both nuclei normally break up, whereas in photoproduction, the photon emitter normally remains intact. Further discussions of the experimental aspects can be found in Reference (91). The conclusion is that sufficient rejection can be obtained with current and planned detectors at heavy-ion colliders to study, e.g., the production of heavy quark pairs.

One significant background to electromagnetic diffraction is hadronic diffraction. Pomeron exchange can also produce rapidity gaps, and double-Pomeron

interactions produce isolated systems in a central detector, with rapidity gaps on each side (100). This is not an issue for vector meson production, because double-Pomeron interactions do not produce $J^{PC} = 1^{--}$ final states, but these backgrounds could be problematic for other reactions. Because the strong force has a short range ($\leq$1 fm), Pomeron exchange between nuclei and double-Pomeron interactions can only occur between surface nucleons in grazing collisions; this limits the cross sections. Unfortunately, quantitative estimates are lacking. However, for pp collisions, Pomeron interactions may constitute a significant background.

Another experimental challenge is finding an efficient trigger with adequate background rejection. Because the outgoing beams are not tagged, it is necessary to trigger on the particles emitted from the final state X in order to study the reaction A+A $\rightarrow$ A+A+X. These particles are usually produced at or near mid-rapidity. Most of the current and planned heavy-ion experiments at RHIC and the LHC have triggers that are optimized for hard, high p_T interactions. These triggers are difficult to adapt to low multiplicity low-p_T final states. STAR at RHIC is an exception, but faces challenges because of the low allowable trigger rates (169). Backgrounds from beam-gas interactions, grazing hadronic collisions, ambient neutrons, and other beam-related backgrounds are serious concerns to any experiment.

In combination with the large probability for multiple Coulomb interactions with heavy beams, factorization has made triggering on neutrons emitted in the forward direction following single or double Coulomb excitation an attractive alternative. This reduces the photon flux, but provides some control of the impact parameter distribution, as discussed in Section 5.

The experimental feasibility of studying ultra-peripheral collisions is demonstrated through the data presented earlier. However, the considerations above limit the types of processes that can be studied. The study of two-photon production of multiple e^+e^--pairs seems difficult because of the extremely low p_T of the emitted electrons. A dedicated experiment would do better, but that is likely to be a difficult proposition at a high-energy physics laboratory. The study of meson spectroscopy at the LHC also seems problematic because of the lack of triggers for low momentum charged particles around mid-rapidity.

7. CONCLUSIONS

We have presented the formalisms for studying photoproduction and two-photon reactions at hadron colliders, and discussed some of the more interesting applications of these techniques. Low-energy nuclear physics has used these techniques for many years, with good results. However, only recently have higher-energy machines like RHIC and the Tevatron begun to study particle production in very strong fields.

The amount of experimental data on UPCs is still rather limited. Despite this, the field has developed tremendously over the past decade, with much theoretical progress. The new data from RHIC is helping to focus new theoretical work on the channels that are most readily accessible. With the new results from RHIC and

the coming LHC startup, UPCs are now ready to make substantial contributions to many areas of physics.

The LHC will produce photonuclear interactions with 10 times the energy available at other accelerators like HERA. This will open a huge window to search for new physics processes (some of them not accessible in hadronic collisions), measure gluon densities at very low Feynman-x, and perform a host of other measurements. At the same time, UPC reactions are very important for machine operations - e^+e^- production with e^- capture will limit the LHC luminosity with heavy ions.

ACKNOWLEDGMENTS

We thank Ramona Vogt for providing Figure 7, Gerhard Baur and Kai Hencken for beneficial discussions, and Heather Gray for helpful comments on the manuscript. This work was supported by the U.S. Department of Energy under grants No. DE-FG02-04ER41338 and DE-AC-03076SF00098.

The *Annual Review of Nuclear and Particle Science* is online at http://nucl.annualreviews.org

LITERATURE CITED

1. Fermi E. *Z. Physik* 29:315 (1924)
2. Marciano W, White S, eds. *Electromagnetic Probes of Fundamental Physics*. Singapore: World Sci. (2003)
3. Weizsäcker CF. *Z. Physik* 88:612 (1934); Williams EJ. *Phys. Rev.* 45:729 (1934)
4. Baur G, Bertulani CA. *Phys. Lett.* B174: 23 (1986)
5. Ritmann JL, et al. *Phys. Rev. Lett.* 70:533 (1993); *Phys. Rev. Lett.* 70:2659 (1993); Schmidt R, et al. *Phys. Rev. Lett.* 70:1767 (1993)
6. Goncalves VP, Bertulani CA. *Phys. Rev. C* 65:054905 (2002)
7. Baur G, et al. *Phys. Lett.* B368:251 (1996)
8. Blanford G, et al. *Phys. Rev. Lett.* 80:3040 (1998)
9. Bertulani CA, Baur G. *Phys. Rep.* 163:299 (1988)
10. Pirner HJ. *Phys. Rev. C* 22:1962 (1980)
11. Feshbach H, Zabek M. *Ann. Phy.* (*NY*) 107:110 (1977); Feshbach H. *Theoretical Nuclear Physics: Nuclear Reactions.* New York: Wiley-InterScience (1993)
12. McLerran L, Venugopalan R. *Phys. Rev. D* 50:2225 (1994)
13. Krauss F, Greiner M, Soff G. *Prog. Nucl. Part. Phys.* 39:503 (1997)
14. Baur G, et al. *Phys. Rep.* 364:359 (2002)
15. Baur G, et al. hep-ex/0201034
16. Baur G, Hencken K, Trautmann D. *J. Phys. G* 24:1657 (1998)
17. Jackson JD. *Classical Electrodynamics*, 2nd ed. New York: Wiley (1975)
18. Baur G, Ferreira Filho LG. *Nucl. Phys.* A518:786 (1990)
19. Vidović M, Greiner M, Best C, Soff G. *Phys. Rev. C* 47:2308 (1993)
20. Drees M, Zeppenfeld D. *Phys. Rev. D* 39: 2536 (1989)
21. Klein S, Nystrand J. *Phys. Rev. Lett.* 92: 142003 (2004)
22. Baur G, et al. *Nucl. Phys.* A729:787 (2003)
23. Ohnemus J, Walsh TF, Zerwas PM. *Phys. Lett.* B 328:369 (1994)
24. Kniehl BA. *Phys. Lett.* B254:267 (1991)
25. Adler C, et al. (STAR Collaboration). *Phys. Rev. Lett.* 89:272302 (2002)

26. Wyatt A. Presented at "Small-x and Diffraction 2003," Fermilab, IL. Transparencies are available at http://conferences.fnal.gov/smallx/new_program.htm
27. Bertulani CA, Canto LF, Hussein MS. *Phys. Rep.* 226:282 (1993)
28. Glasmacher T. *Annu. Rev. Nucl. Part. Sci.* 48:1 (1998)
29. Aumann T, Bortignon PF, Emling H. *Annu. Rev. Nucl. Part. Sci.* 48:351 (1998)
30. Bertulani CA, Ponomarev V Yu. *Phys. Rep.* 321:139 (1999)
31. Hansen PG, Jensen AS, Jonson B. *Annu. Rev. Nucl. Part. Sci.* 45:591 (1995)
32. Bertulani CA, Hussein M, Muenzenberg G. *Physics of Radioactive Beams.* Hauppage, NY: Nova Science (2002)
33. Jonson B. *Phys. Rep.* 389:1 (2004)
34. Alder K, et al. *Rev. Mod. Phys.* 28:432 (1956)
35. Clayton DD. *Principles of Stellar Evolution and Nucleosynthesis.* New York: McGraw-Hill (1968)
36. Rolfs C, Rodney WS. *Cauldrons in the Cosmos* Chicago: Univ. Chicago Press (1988)
37. Baur G, Bertulani CA, Rebel H. *Nucl. Phys.* A458:188 (1986)
38. Schuemann F, et al. *Phys. Rev. Lett.* 90: 232501 (2003)
39. Hammache F, et al. *Phys. Rev. Lett.* 86:3985 (2001); Junghans AR, et al. *Phys. Rev. Lett.* 88:041101 (2002); Baby LT, et al. *Phys. Rev. Lett.* 90: 022501 (2003); *Phys. Rev. C* 67:065805 (2003)
40. Baur G, Rebel H. *Annu. Rev. Nucl. Part. Sci.* 46:321 (1996); Baur G., Hencken K, Trautmann D. *Prog. Part. Nucl. Phys.* 51: 487 (2003)
41. Goldhaber M, Teller E. *Phys. Rev.* 74: 1046 (1948)
42. Steinwedel H, Jensen JHD. *Z. Naturforsch.* 5a:413 (1950)
43. Ritman J, et al. *Phys. Rev. Lett.* 70:533 (1993)
44. Schmidt R, et al. *Phys. Rev. Lett.* 70:1767 (1993)
45. Aumann T, et al. *Phys. Rev. C* 47:1728 (1993)
46. Boretzky K, et al. *Phys. Lett.* B384:30 (1996)
47. Grünschloss A, et al. *Phys. Rev. C* 60:051601 (1999)
48. Boretzky K, et al. *Nucl. Phys.* A649:235c (1999)
49. Ilievski S, et al. *Nucl. Phys.* A687:178c (2001)
50. Bertulani CA, Canto LF, Hussein MS, de Toledo Piza AFR. *Phys. Rev. C* 53:334 (1996)
51. Hussein MS, de Toledo Piza AFR, Vorov OK. *Phys. Rev. C* 59:R1242 (1999)
52. de Toledo Piza AFR, et al. *Phys. Rev. C* 59:3093 (1999); Carlson BV, et al. *Phys. Rev. C* 59:2689 (1999); Carlson BV, Hussein MS. *Phys. Rev. C* 59:R2343 (1999); Carlson BV, Hussein MS, de Toledo Piza AFR, Canto LF. *Phys. Rev. C* 60:014604 (1999)
53. de Paula DT, et al. *Phys. Rev. C* 64:064605 (2001)
54. Pshenichnov IA, et al. *Phys. Rev. C* 64: 024903 (2001)
55. Baltz AJ, et al. *Phys. Rev. E* 54:4233 (1996); Baltz AJ, Chasman C, White SN. *Nucl. Instrum. Meth. A*, 417:1 (1998); White SN. *Nucl. Instrum. Meth. A* 409:618 (1998)
56. Chiu M, et al. *Phys. Rev. Lett.* 89:012302 (2002)
57. Bertulani CA, Baur G. *Physics Today* 22: March (1994)
58. Hoffman B, Baur G. *Phys. Rev. C* 30:247 (1984)
59. Klein S, Vogt R. *Phys. Rev. C* 68:017902 (2003)
60. White SN. nucl-ex/0501004.
61. Gousset T, Pirner HJ. *Phys Lett. B* 375:349 (1996)
62. Eskola KJ, Kolhinen VJ, Ruuskanen PV. *Nucl. Phys. B* 535:351 (1998)
63. Frankfurt L, Strikman M. *Eur. Phys. J.* A5:293 (1999)
64. Bauer TH, Spital RD, Yennie DR. *Rev. Mod. Phys.* 50:261 (1978)

65. Crittenden JA. *Exclusive Production of Neutral Vector Mesons at the Electron-Proton Collider HERA*. Berlin: Springer-Verlag (1997)
66. Schuler GA, Sjöstrand T. *Nucl. Phys.* B 407:539 (1993)
67. Pautz A, Shaw G. *Phys. Rev. C* 57:2648 (1998)
68. Klein S, Nystrand J. *Phys. Rev. C* 60: 014903 (1999)
69. Frankfurt L, Strikman M, Zhalov M. *Phys. Lett.* B540:220 (2002)
70. Glauber RJ. In *Lectures in Theoretical Physics*, ed. WE Britten, LG Dunham. New York: Interscience (1959)
71. Grammer G, Sullivan JD. In *Electromagnetic Interactions of Hadrons*, Vol. 2, ed. A Donnachie, G Shaw. New York and London: Plenum (1978)
72. Alberi G, Goggi G. *Phys. Rep.* 74:1 (1981)
73. Frankfurt L, Strikman M, Zhalov M. *Phys. Lett.* B537:51 (2002)
74. Frankfurt L, Strikman M, Zhalov M. *Phys. Rev. C* 67:034901 (2003)
75. Meissner F (for the STAR Collaboration). *Nucl. Phys.* A715:522c (2003)
76. Baltz AJ, Klein SR, Nystrand J. *Phys. Rev. Lett.* 89:012301 (2002)
77. Söding P. *Phys. Lett.* 19:702 (1966)
78. Timoshenko SL (for the STAR Collaboration). nucl-ex/0501010
79. Ogawa A (for the STAR Collaboration). Presented at DIS2004, April 14–18, 2004, Strbske Pleso, Slovakia
80. Silvermyr D (for the PHENIX Collaboration). Presented at DNP04, Meeting of the Nucl. Phys. Div. of the APS, Chicago, Oct. 27–30, 2004. http://www.phenix.bnl.gov/conferences.html
81. Ryskin MG. *Z. Phys. C* 57:89 (1993)
82. Frankfurt LL, McDermott MF, Strikman M, *J. High Energy Physics* 02:002 (1999)
83. Martin AD, Ryskin MG, Teubner T *Phys. Lett.* B454:339 (1999)
84. Klein SR, Nystrand J. *Phys. Rev. Lett.* 84: 2330 (2000); *Phys. Lett.* A308:323 (2003)
85. Baur G, Ferreira-Filho LG. *Phys. Lett.* B 254:30 (1991)
86. Klein SR (for the STAR Collaboration). nucl-ex/0310020; nucl-ex/0402007
87. Pshenichnov IA, et al. *Phys. Rev. C* 60: 044901 (1999)
88. Nystrand J, Klein S. *nucl-ex/9811007* (1998), *Proc. Workshop on Photon Interactions and the Photon Structure*, eds. G. Jarlskog, T. Sjöstrand, Lund, Sweden, Sept. (1998)
89. Greiner M, et al. *Phys. Rev. C* 51:911 (1995)
90. Klein SR, Nystrand J, Vogt R. *Eur. Phys. J. C* 21:563 (2001)
91. Klein SR, Nystrand J, Vogt R. *Phys. Rev. C* 66:044906 (2001)
92. Goncalves VP, Machado MVT. *Phys. Rev. D* 71:014025 (2005); *Eur. Phys. J.* C40:519 (2005)
93. Jones LM, Wyld HW. *Phys. Rev. D* 17:759 (1978)
94. Fritzsch H, Streng KH. *Phys. Lett.* B72:385 (1978)
95. Smith J, van Neerven WL. *Nucl. Phys.* B 374:36 (1992)
96. Baur U, Buice M, Orr LH, *Phys. Rev. D* 64:094019 (2001)
97. Frankfurt L, Guzey V, Strikman M. hep-ph/0303022
98. Vogt R. hep-ph/0407298
99. Frankfurt L, Strikman M. *Phys. Rev. D* 67:017502 (2003)
100. Eggert K, et al. *FELIX Letter of Intent, CERN/LHCC 97/45;* Ageev, et al. *J. Phys. G* 28:R117 (2002); Engel R, Ranft J., Roesler S. *Phys. Rev. D* 55:6957 (1997)
101. Pumplin J. hep-ph/9612356
102. Furry WH, Carlson JF. *Phys. Rev.* 44:238 (1933)
103. Landau LD, Lifshitz EM. *Phys. Zs. Sowjet* 6:244 (1934)
104. Bhabha HJ. *Proc. R. Soc. London Ser. A* 152:559 (1935)
105. Nishina Y, Tomonaga S, Kobayashi M. *Sci. Pap. Phys. Chem. Res.* 27:137 (1935)
106. Racah G. *Nuovo Cimento* 14:93 (1937)
107. Antreasyan D, et al. preprint CERN-EP/80–82 (1990)

108. Morgan D, Pennington MR, Whalley MR, *J. Phys. G* 20:A1 (1994)
109. Low FE. *Phys. Rev.* 120:582 (1960)
110. Baur G, Bertulani CA. *Z. Phys. A* 330:77 (1988); Bertulani CA, Baur G. *Nucl. Phys.* A505:835 (1989)
111. Yang CN. *Phys. Rev.* 77:242 (1950); Wolfenstein L and Ravenhall DG. *Phys. Rev.* 88:279 (1952)
112. Bodwin GT, Yennie DR, Gregorio MA *Rev. Mod. Phys.* 57:723 (1985)
113. Sapirstein J, Yennie DR. In *Quantum electrodynamics*, ed. T. Kinoshita. Singapore: World Sci. (1990)
114. Kotkin GL, Kuraev EA, Schiller A, Serbo VG. *Phys. Rev. C* 59:2734 (1999)
115. Bertulani CA, Navarra F. *Nucl. Phys.* A703:861 (2002)
116. Nemenov LL. *Yad. Fiz.* 51:444 (1990); *Sov. J. Nucl. Phys.* 51:284 (1990); Lyuboshitz VL, Podgoretsky MI. *Zh. Eksp. Teor. Fiz.* 81:1556 (1981)
117. Appelquist T, Politzer HD. *Phys. Rev. Lett.* 34:43 (1975)
118. Baur G. *Phys. Rev. D* 41:3535 (1990); *Phys. Rev. A* 42:5736 (1990)
119. Bottcher C, Strayer MR. *Phys. Rev. D* 39:1330 (1989); *J. Phys. G* 16:975 (1990); *Phys. Lett.* B237:175 (1990)
120. Rhoades-Brown MJ, Weneser J. *Phys. Rev. A* 44:330 (1991)
121. Best C, Greiner W, Soff G. *Phys. Rev. A* 46:261 (1992)
122. Hencken K, Trautmann D, Baur G. *Phys. Rev. A* 51:998 (1995); *Phys. Rev. A* 51:1874 (1995)
123. Lee RN, Milstein AI, Serbo VG. *Phys. Rev. A* 65:022102 (2002)
124. Güçlü MC. *Nucl. Phys.* A668:149 (2000)
125. Ivanov DY, Schiller A, Serbo VG. *Phys. Lett.* B 454:15 (1999)
126. Lee RN, Milstein AI. *Phys. Rev. A* 61:032103 (2000); *Phys. Rev. A* 64:032106 (2001)
127. Aste A, et al. *Eur. Phys. J. C* 23:545 (2002)
128. Bartos E, Gevorkyan SR, Kuraev EA, Nikolaev NN. *Phys. Lett.* B538:45 (2002)
129. Eichler J, Meyerhof W. *Relativistic Atomic Collisions.* San Diego: Academic (1995)
130. Baltz AJ. *Phys. Rev. Lett.* 78:1231 (1997)
131. Baltz AJ, McLerran L. *Phys. Rev. C* 58: 1679 (1998)
132. Segev B, Wells JC. *Phys. Rev. A* 57:1849 (1998); *Phys. Rev. C* 58:1697 (1998)
133. Eichmann U, Reinhardt J, Schramm S, Greiner W *Phys. Rev. A* 59:1223 (1999)
134. Hencken K, Trautmann D, Baur G. *Phys. Rev. A* 59:841 (1999)
135. Eichmann U, Reinhardt J, Greiner W. *Phys. Rev. A* 61:062710 (2000); *Phys. Rev. C* 61:064901 (2000)
136. Hencken K, Baur G, Trautmann D. *Phys. Rev. C* 69:054902 (2004)
137. Baltz AJ, Gelis F, McLerran L, Peshier A. *Nucl. Phys. A* 695:395 (2001)
138. Baltz AJ, Rhoades-Brown MJ, Weneser J. *Phys. Rev. A* 44:5569 (1991); *Phys. Rev. A* A48:2002 (1993); *Phys. Rev. A* 47:3444 (1993); *Phys. Rev. A* 50:4842 (1994)
139. Baltz AJ. *Phys. Rev. A* 52:4970 (1995)
140. Bertulani CA. *Phys. Rev. A* 63:062706 (2001)
141. Baltz AJ. nucl-th/0409044
142. Adams J, et al. *Phys. Rev. C* 70:031902 (2004)
143. Baur R, et al. *Phys. Lett.* B332:471 (1994)
144. Vane CR, et al. *Phys. Rev. A* 50:2313 (1994)
145. Klein S. *Nucl. Instrum. Meth. A* 459:51 (2001)
146. Brandt D. *LHC Project Report 450.* www.cern.ch (2000)
147. Bertulani CA, Baur G. *Phys. Rev. D* 58:034005 (1998)
148. Bertulani CA, Dolci D. *Nucl. Phys.* A683:635 (2001)
149. Anholt R, Becker U. *Phys. Rev. A* 36:4628 (1987)
150. Becker U. *J. Phys. B* 20:6563 (1987)
151. Bottcher C, Strayer MR. *J. Phys. G* 16:975 (1990); *Phys. Lett.* B237:175 (1990)
152. Meier H, et al. *Phys. Rev. A* 63:032713 (2001)

153. Krause HF, et al. *Phys. Rev. Lett.* 80:1190 (1998)
154. Scheidenberger C, et al. *Phys. Rev. Lett.* 88:042301 (2002); *Phys. Rev. C* 70:014902 (2004)
155. Pshenichnov IA, et al. *Phys. Rev. C* 57:1920 (1998); *Phys. Rev. C* 64:024903 (2001)
156. Geer LY, et al. *Phys. Rev. C* 52:334 (1995)
157. Cahn RN, Jackson JD. *Phys. Rev. D* 42:3690 (1990)
158. Khoze VA, Martin AD, Ryskin MG. *Eur. Phys. J. C* 23:311 (2002)
159. Vidovic M, Greiner M, Soff G. *Phys. Rev. C* 47:2288 (1993)
160. Piotrzkowski K. *Phys. Rev. D* 63:071502 (2001)
161. Abbott B, et al. *Phys. Rev. Lett.* 81:524 (1998)
162. Ahern SC, Norbury JW, Poyser WJ. *Phys. Rev. D* 62:116001 (2000)
163. Papageorgiu E. *Phys. Rev. D* 40:92 (1989)
164. Grabiak M, Müller B, Greiner W, Koch P. *J. Phys. G* 15:L25 (1989)
165. Drees M, Ellis J, Zeppenfeld D. *Phys. Lett.* B223:454 (1989)
166. Nikulin V. Presented at 2nd Workshop on Ultra-Peripheral Heavy Ion Collisions, Oct. 11–12, 2002, CERN, Geneva
167. Baur G, Hencken K, Trautmann D, Sadovsky S and Kharlov Y. e-Print Archive hep-ph/990436
168. Gupta SN. *Phys. Rev.* 99:1015 (1955)
169. Bieser FS, et al. *Nucl. Instrum. Meth. A* 499:766 (2003)
170. S. Eidelman, et al. (Particle Data Group), *Phys. Lett.* B592:1 (2004)

Annual Review of Nuclear and Particle Science
Volume 55, 2005

CONTENTS